FLOW IN A DIVERGING TUBE

DZHELIL S. RUFAT

May 19, 2006

Submitted to

the Department of Engineering Science,

University of Oxford

Final Report

Advisor: Dr Yiannis Ventikos

47 pages

ABSTRACT. Branching plays a major role in the human respiratory and cardiovascular system. In this paper we model branching vessels in the human body as pipes merging at a junction and numerically investigate the role of the bifurcation on the flow.

Various geometries with bifurcation angles of 90°,120°, 150° and 180°, mother-to-daughter tube diameter ratios of 1/2 and 1, and inlet flow Reynolds numbers of 200, 400 and 600 are considered. In addition to velocity profile across the cross-section, shear stress and advective mixing is studied. The axial velocity field in each daughter tube is found to contain sharp peak, which has a very steep velocity gradient near the inside walls and a flat profile near the outside walls, thus leading to a high shear stress on the inside splitting walls and lower shear stress on the outside wall. Secondary flow pattern in each daughter tube consist of two vortices, which are similar to the Dean vortices in a curved pipe.

Advective mixing describing how massless particles would be advected through the flow is also computed. It turns out that the advective mixing moves the central region at the inlet to the peripheral regions of the outlet, indicating that bifurcations may play an important role in the exchange between the fluid and the vessel walls.

Figures are provided showing the mixing across several successive bifurcations.

To validate the computational model grid independence studies are carried.

Contents

1. Introduction

Branching of fluid flows is extremely common within the human body, especially in the cardiovascular system and within the lungs, and involves many different geometrical configurations and flow conditions of varying Reynolds numbers,pulsatility and wall flexibility.

Systems where branching plays an important role are usually involved in the transport of nutrients, waste and respiratory gases. Lungs accomplish this function through a complex system of branching tubes forming a bronchial tree, whereas the cardiovascular system does it through an internal flow loop with multiple branches within which a complex liquid circulates. Regardless of the different nature of the two systems, in both branching play an important role and any understanding of the flow requires a discussion of the mechanism by which bifurcations exert a downstream influence on the flow. Understanding this mechanism is key to gaining more insight about the relationship between local hemodynamics in bifurcation and vascular disease. Portions of the vascular wall exposed to disturbed flow, such as the regions of high curvature and bifurcations are prone to the formation of atherosclerosis.

Tadjfar [12] has computed the flow and the shear-stress distribution for a single branching. In a different paper [13] the same author has also studied analytically a three-dimensional bifurcating tube where the daughter tube has a semi-circular cross-section.

The role of bifurcations within the human airways which form a rapidly diverging system of branching tubes has been studied by Pedley [6].

Smith [10] has extended previous work of one-to-two branching to one-to-many tubes.

Understanding the flow within vascular and bronchial tracts of interest is rendered nontrivial by the complex topology and hemodynamics. The complexity of the problem compels us to make several simplifying assumptions at the outset. All tubes are assumed to be straight circular pipes with smooth rigid walls on which the no slip condition is imposed. The blood is assumed to be a Newtonian fluid with a fixed viscosity. The assumption of unsteady flow is probably the most significant limitation in this study limiting its applicability to physiological flows. Nonetheless, this work gives us important insights the flow especially in cases where the unsteadiness has little effect to fluid dynamics in comparison to the local geometry.

This investigation concentrates on a basic symmetric branching flow, the branching being from one mother tube to two daughter tubes downstream neglecting all effects of pulsatility, rheological blood characteristics and wall deformability.

A qualitative picture of the flow in a branching tube with a maximal velocity on the axis of the mother tube can be given by separating the phenomena that influence the flow into two main parts.

The first part is due to the fact that the flow is divided into two streams and a growing boundary layer is formed on the inside wall of the daughter tube with the velocity reaching its peak value very close to the internal splitting wall - this will be referred to as the splitting effect. The second effect is related to curvature and occurs since the flow turns a corner and moves in a curved pipe. A centrifugal instability arises because the inertia of the faster moving fluid pushes it away from the bend, the axial velocity profile is shifted towards the internal wall of the pipe (i.e. away from the bend) and a secondary flow pattern typical of Dean flow emerges. This flow effect will be called the curvature effect. Understanding the combined influence on the flow of these two effects requires one to look into them separately, since the observed flow will be a complex superposition of these two flow patterns.

Separate investigations of these two effects have been carried out before by various authors and approximate analytic solutions of the flow has been found. In this study we merge these two effects and manifestations of both of them will be visible in our solution.

The curvature effect has been studied both analytically and numerically within a bending pipe with small [1], finite [9], varying [5] curvature. The splitting effect for a high Reynolds number flow through a circular plane split along the diameter by a semi-infinite splitter plain is considered by Blyth and Mestel [2] as an approximation to a bifurcation of angle zero. The flow has been analyzed using a matched asymptotic expansion by dividing the flow into four regions. Unlike Blyth's approximation to a zero angle in this work we mainly consider bifurcations with an obtuse angle and therefore our work can be considered an extension to his small angle bifurcations.

The flow (i.e. the velocity field) at any point will depend on a number of parameters - the location of the point, the Reynolds number, the mother to daughter tube diameter ratio, the angle of bifurcation, the local geometry of the junction and its curvature, and finally the conditions downstream of the bifurcation.

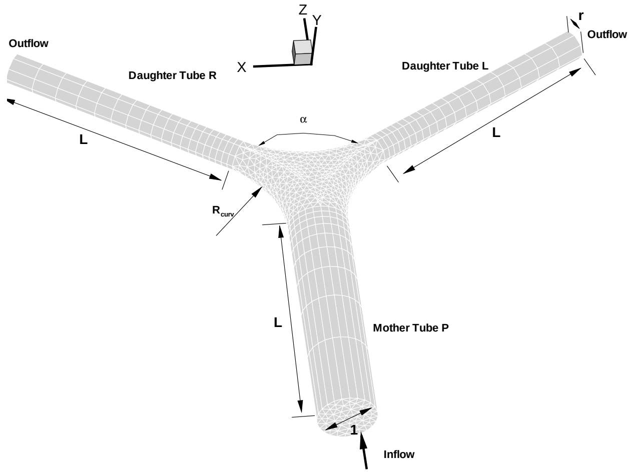

FIGURE 1. Bifurcation Geometry

In this study we will solve the Navier-Stokes equation for bifurcations with various geometries and various values for the above parameters. We will compute the mixing over one and several generations of bifurcations, and finally the shear stress will be studied as well since it is known that bifurcations are preferential sites for atherosclerosis.

2. Problem Formulation

The three dimensional laminar steady flow of incompressible Newtonian viscous fluid through a straight mother tube bifurcating into two symmetrically divergent daughter tubes of circular cross-section is considered.

2.1. Governing Equation and Non-dimensionalizing the Problem. It is convenient to use the Navier-Stokes equation in non-dimensional units. Then the diameter and velocity can be set to 1 and for a given geometry the flow will be associated with a unique Reynolds number.

In dimensional form Navier-Stokes equation and the continuity equation (for an incompressible fluid) are well known

$$\rho(\frac{\partial v}{\partial t} + v \cdot \nabla v) = -\nabla p + \mu \nabla^2 v + \rho g \tag{1}$$

$$\nabla \cdot v = 0 \tag{2}$$

Now let us non-dimensionalize the above equation in terms of the following flow parameters

$$\Psi = \frac{L_c^2 \rho}{\mu T_c} \tag{3}$$

$$Re = \frac{\rho L_c U_c}{\mu} \tag{4}$$

$$Fr = \frac{U_c}{\sqrt{g L_c}} \tag{5}$$

where L_c, T_c and $U_c = \frac{L_c}{T_c}$ are the characteristic length, time and velocity of the problem respectively. Ψ is a measure of the unsteadiness and Fr is a measure of the relative importance of gravity. Re is the Reynolds number which measure the balance between the inertial and viscous forces.

Let $v \rightarrow \frac{v}{U_c}$, $x \rightarrow \frac{x}{L_c}$, $t \rightarrow \frac{t}{T_c}$ $p \rightarrow \frac{p}{\rho U_c^2}$. Then we arrive at the non-dimensional form of the Navier-Stokes equation:

$$\frac{\Psi}{Re}\frac{\partial v}{\partial t} + v \cdot \nabla v = -\nabla p + \frac{1}{Re}\nabla^2 v + \frac{1}{Fr^2}\hat{g} \tag{6}$$

where $\hat{g}$ is a unit vector pointing in the direction of the gravitational field.

In this study we will be dealing with steady flows ($\Psi = 0$) where the effect of gravity plays a negligible role locally ($Fr = 0$) and then the Navier-Stokes momentum transfer equation is simplified to:

$$(v \cdot \nabla)v = -\nabla p + \frac{1}{Re}\nabla^2 v \tag{7}$$

$$\nabla \cdot v = 0 \tag{8}$$

This is the Navier-Stokes equation in its general invariant form, with the conventional dot product in Cartesian coordinates. Often non-Cartesian coordinates are more appropriate, and it is therefore better to express the equation in a general curvilinear coordinate system, and then the Navier-Stokes equation will read:

$$v^k v^i_{\ ;k} = -g^{ik} p_{;k} + \nu g^{jk} v^i_{\ ;jk} \tag{9}$$

$$v^i_{\ ;k} = 0 \tag{10}$$

where ${v^i}_{;j}$ denotes the covariant derivative given by

$$(11) \qquad {v^i}_{;j} = {v^i}_{,j} + \Gamma^i_{jk} v^k, \qquad \Gamma^i_{jk} = \frac{1}{2} g^{im} (g_{mj,k} - g_{jk,m} + g_{km,j})$$

g is the metric tensor.

The tensor form of the Navier-Stokes equation in a curved coordinate system is useful since often the coordinate system used is a curvilinear one (for instance in the case of a pipe it is convenient to work in cylindrical coordinates). Many difficult problems have been solved in a perturbation series for small curvatures by expanding around a known solution. A typical example is the derivation of the Dean flow in a curved pipe as a perturbation series around Poiseuille flow in a straight pipe. See Appendix A for more details.

2.2. **Boundary Conditions.** Let ξ describe the position across the inlet, and χ the position across any of the outlet.

We assume a parabolic profile at the inlet

$$(12) \qquad \vec{v}(\xi) = \left[0, 0, 1 - \frac{\xi^2}{4} \right]$$

and a constant pressure gradient across the cross-section of the inlet and the outlet $\frac{\partial p}{\partial \xi} = \frac{\partial p}{\partial \chi} = 0$ and the no slip condition is enforced on the tube walls.

All parameters in this problem have been non-dimensionalized as described in the last section, where the characteristic length is taken as the diameter of the mother tube, and the characteristic velocity is the maximal axial velocity in the mother tube. Then the Reynolds number will be the only flow parameter, in addition to those defining the geometry,

$$(13) \qquad Re = \frac{\rho v_{max} D}{\mu} = \frac{\rho \bar{v} R}{\mu}$$

where $\bar{v}$ is the mean velocity and $R = D/2$ is the radius.

It is evident that the velocity field must satisfy the following symmetries.

$$R_1 : (x, y, z) \to (-x, y, z) : (u, v, w) \to (u, v, w)$$

$$(14) \qquad R_2 : (x, y, z) \to (x, -y, z) : (u, v, w) \to (u, v, w)$$

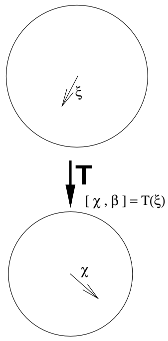

FIGURE 2. Stream map

These symmetries will be manifest in our solutions, although in general they cannot be used to confirm grid-independence since there are steady flows in which bistable and not necessarily symmetric solutions may arise even with symmetric geometries and boundary conditions.

2.3. **Wall Shear Stress Calculation.** A flow quantity of particular interest in this investigation is the wall shear stress defined on a surface with a normal $n = [n_1, n_2, n_3]$ as follows

$$\tau_i = \mu(\partial_i v_j + \partial_j v_i)n_j \qquad \tau_i = \frac{1}{Re}(\partial_i v_j + \partial_j v_i)n_j \tag{15}$$

2.4. **Transfer Function.** Every streamline connects a point from the inlet to a point on the outlet and therefore defines a mapping $T : \xi \to \chi$ (Figure 2) which we will call the Stream Transfer Function. Derivation of the transfer function requires computing the streamlines and a knowledge of the velocity everywhere within the computational domain is necessary.

A stream line is a curve described by $\sigma(t) \in \mathcal{R}^3$ and satisfying the condition that it is tangent to the velocity field everywhere

$$\frac{d}{dt}\sigma(t) = v(\sigma(t)) \tag{16}$$

From this defining differential equation it is evident that integrating the velocity along the streamline must result in the streamline itself, and we deduce that a streamline must satisfy an integral equation, where the unknown function $\sigma(t)$ appears both inside and outside of the integral sign

$$\sigma(t) = \int_0^t dt' v(\sigma(t')) \tag{17}$$

The integral definition is more convenient when dealing with complicated velocity fields because it allows us to design an iterative technique to evaluate the stream lines. Starting with an initial guess function $\sigma_0(t)$ we can integrate the velocity along that line, and obtain a new stream line which hopefully will be a better approximation to the actual streamline.

$$\sigma_n(t) = \int_0^t dt' v(\sigma_{n-1}(t')) \tag{18}$$

If there exists a limit for this recursive equation, then it must converge to the actual solution $\sigma_n \to \sigma$ when $n \to \infty$.

A streamline defines a one-to-one correspondence between a point on the inlet and a point in the outlet, and hence the stream transfer function from a point ξ at the inlet to a point χ at the outlet $T(\xi) = [\chi, \beta]$ where

$$\xi = \sigma(0) \qquad \chi = \sigma(\infty) \tag{19}$$

and β is a discrete variable which determines in which outlet the streamline ends up

$$\beta(\xi) = \begin{cases} 0, & \xi_1 < 0 \quad \text{left outlet} \\ 1, & \xi_1 > 0 \quad \text{right outlet} \end{cases} \tag{20}$$

β is undefined on on the splitting line $\xi_1 = 0$ since streamlines that start there are prematurely terminated on the splitting wall of the bifurcation before they reach the outlets.

Deriving analytically an expression for the transfer function is a hopelessly difficult task in the case of the complex bifurcation geometry we have, so we will only derive it numerically in this work by integrating the streamlines numerically along the discrete velocity field. Nevertheless, the technique for the derivation of T described in this section can be of use for other, simpler geometries. Although somewhat irrelevant to the bifurcation geometry considered in this investigation, as an illustrative example of the power of the above recursive technique the stream transfer function is computed for a gently curving pipe to first order in the curvature in Appendix A.

3. Numerical Method

The first step before the numerical simulations is to define and discretize the computational domain and for this purpose the commercial software package CFG-GEOM by CFD Research Corporation has been used. CFD-GEOM supports the scripting language Python and all the geometry and mesh operations are accessible from Python script language, making it possible to write custom parametric script templates. The whole procedure for the generation of the geometry and the meshing has been fully automated. The code used to generate the geometry and the mesh is included for the reader's convenience in Appendix B in case an exact duplication of the geometries in this paper is necessary.

3.1. **Geometry.** As shown on Figure 1 the model consists of a mother tube of circular cross-section and a unit diameter, and two daughter tubes, which apart from the region of local adjustment near the bifurcation point, are also of circular cross-sections with a diameter r. The axes of all the tubes are coplanar in the xz-plane. The angle subtended by the axes of the left and right daughter tubes is α. Our interest in this paper will be to study how the angle α affects the flow.

The radius of curvature R_{curv} is another parameter, which adds an extra degree of freedom to the bifurcation geometry and it determines how sharply the daughter tubes bend away from the mother tube.

Figure 3 illustrates step by step the creation of the geometry and the incorporation of each parameter into the geometry. First, start with a single circle of unitary diameter representing the cross-section of the mother tube (a). From the two diametrically opposed points of the circle extrude two diverging arcs of radius R_{curv} and length $\frac{\alpha}{2}R_{curv}$ (b). At each of the endpoints of the arcs attach orthogonally two circles of diameter r representing the cross-sections of the daughter tubes. Extrude all of the three circles by a length L(c). This essentially defines the skeleton of the geometry. It remains to define the surface geometry of the bifurcation and to map the output of the mother tube to the two inputs of the daughter tubes. For this the blending curve function of CFD-GEOM which smoothly connects two lines by fitting a fourth-order polynomial between the selected endpoints, is employed. For each daughter tube two blending curves are necessary to blend the top and the bottom to the mother tube, and three more are necessary to blend the daughter tube to each other yielding the geometry skeleton as shown in (d). It is now easy to patch the skeleton with smooth 4-sided and 3-sided surfaces.

The radius of curvature is a parameter that only affects the geometry of the bifurcation region, and for this reason it would be convenient to isolate it and express it in terms of the other parameters of the geometry. A convenient choice is

$$R_{curv} = \frac{\frac{1}{2} + r\cos\frac{\alpha}{2}}{1 - \cos\frac{\alpha}{2}} \tag{21}$$

.

This choice ensures that the distance between the inlets of the two daughter tubes is always equal to 2, and only affects the geometry of the bifurcation region, the length of the straight sections is unaffected. This of course is an arbitrary choice which make the geometry look nice for obtuse angles, and for a different range of angles a different choice might be more appropriate.

3.2. **Mesh.** Having defined the surface we proceed with its discretization. The finite volume mesh is shown on Figure 3 An unstructured tetrahedral mesh is used for the region of the bifurcation, and the straight section of each pipe is built up from triangular prism elements whose height is appropriately stretched near the ends to save computational time.

The discretization procedures consists of three steps.

- Skeleton Discretization Define δ is a characteristic length parameter describing the fineness of the mesh. Then we divide each line segment of the skeleton into the following number of collocation points:

$$N = 1/\delta \tag{22}$$

$$N_A = \pi r/\delta \tag{23}$$

$$N_P = \pi/\delta \tag{24}$$

$$N_L = L/\delta \tag{25}$$

$$N_O = \frac{\alpha}{2} R_{curv}/\delta \tag{26}$$

$$N_I = \frac{\alpha}{2}(R_{curv} + \frac{1}{2})/\delta \tag{27}$$

$$N_S = 2\left(R_{curv} + \frac{1}{2} - \cos\frac{\alpha}{2}(R_{curv} + r)\right)/\delta \tag{28}$$

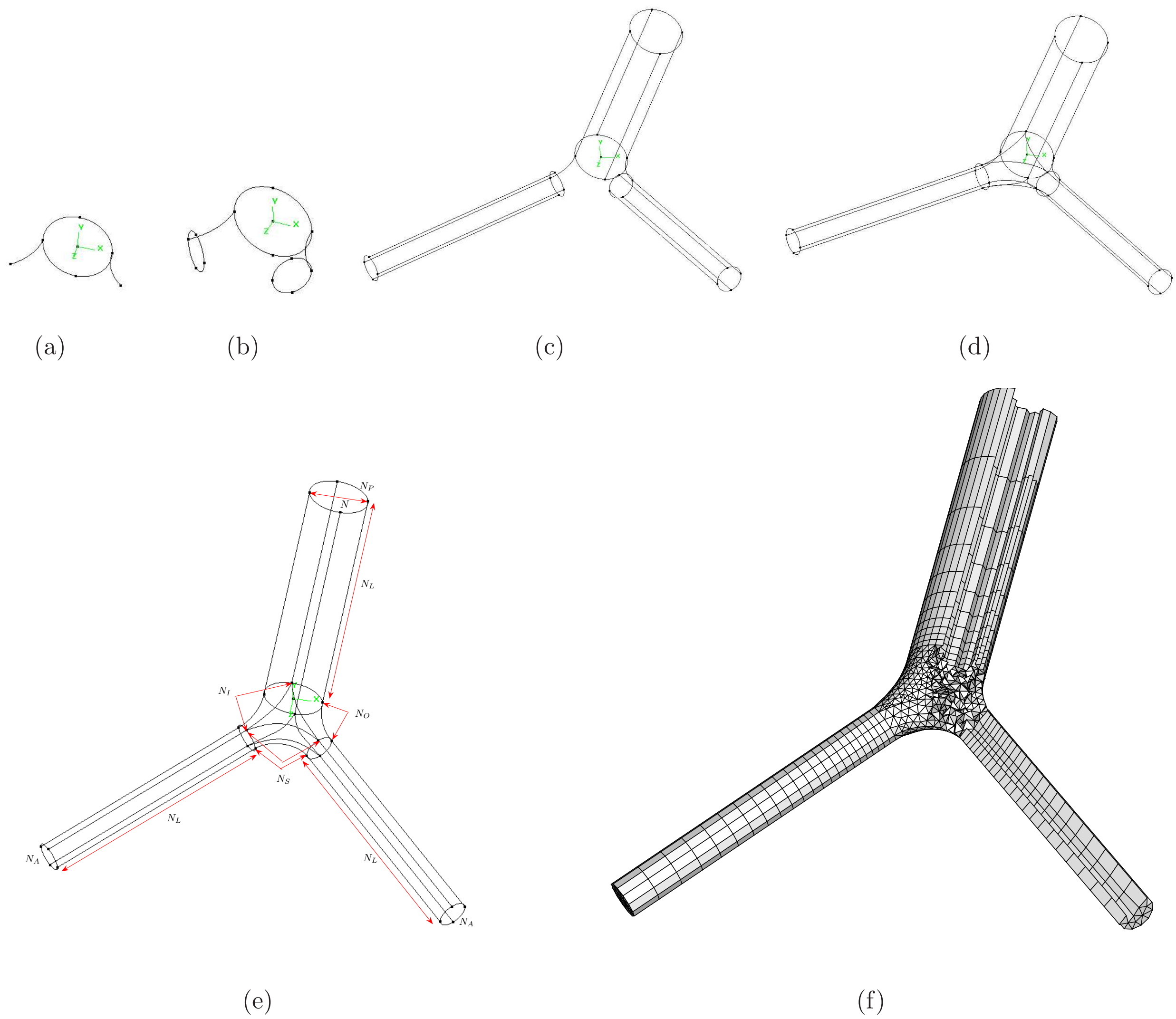

FIGURE 3. Step-by-step generation of the surface geometry and the finite volume mesh. Part of the mesh has been removed to show the unstructured finite-volume discretization.

Here N is the number of elements across the parameters, and the rest of the notation is explained on Figure 3. In choosing these numbers we have tried to ensure that the length scale is roughly the same all over the computational domain, and that the smallest elements are located in the junction region where we observe high gradients of the velocity and pressure fields, and that the biggest elements are located at the exit of each pipe where we expect the flow to be fully-developed.

- Triangulation The surface triangulation is generated using CFD-GEOM with an expansion parameter of 1.01.

- Tetrahedra and Prism Generation The tetrahedral mesh in the bifurcation region is generated using the functionality of the CFD-GEOM with an expansion parameter of 1.01. The prism mesh in the straight sections is created by extruding the triangular surface mesh from the input and outputs of the bifurcation region.

3.3. **Flow Solver.** For the numerical solution of flow in a bifurcating pipe the commercial finite volume method based Navier-Stokes solver CFD-ACE, by CFD Research Corporation, has been used. The convergence has been accelerated by the employing the algebraic multigrid acceleration.

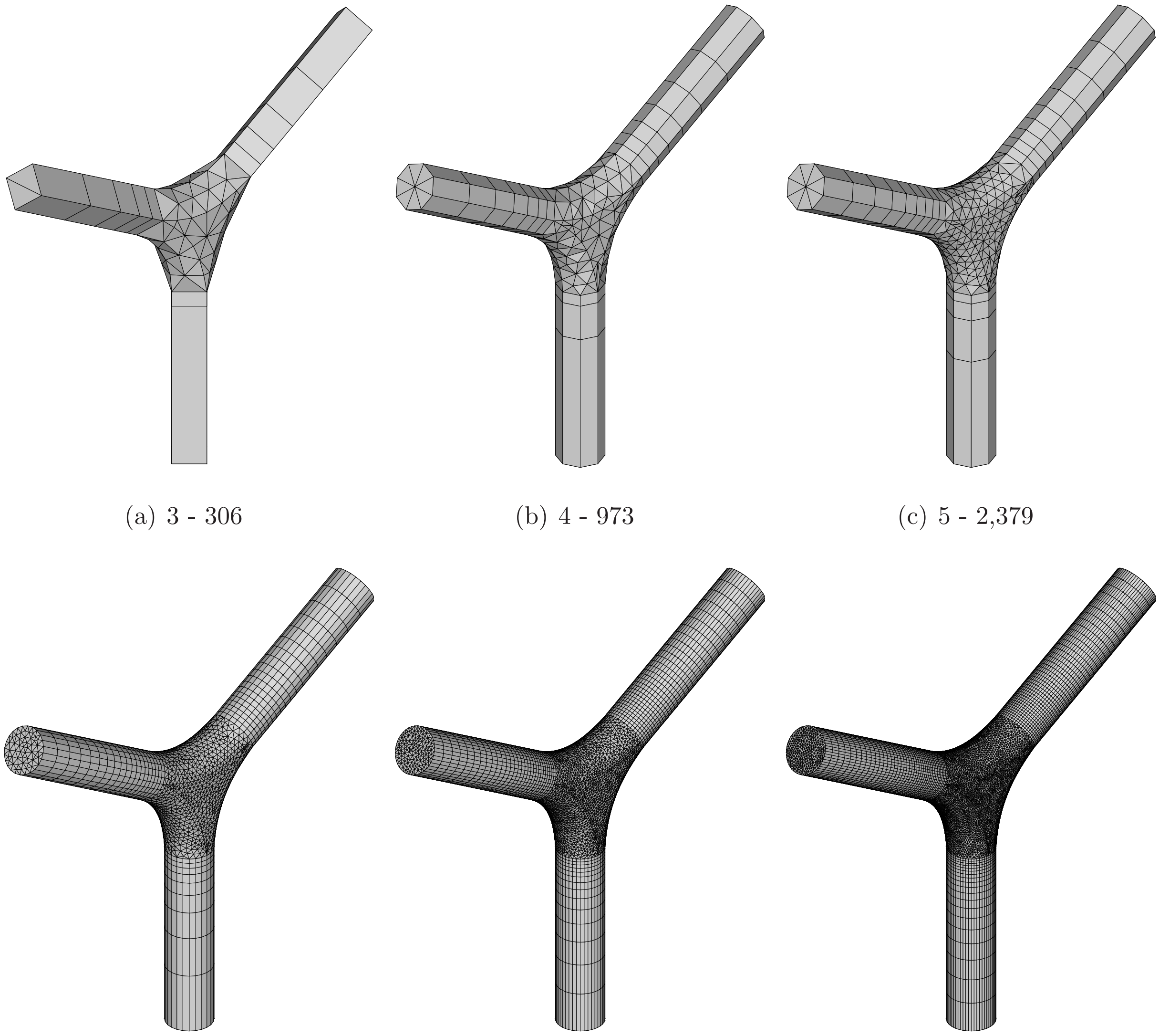

(a) 3 - 306 (b) 4 - 973 (c) 5 - 2,379

(d) 10 - 26,968 (e) 15 - 96,197 (f) 20 - 230,517

FIGURE 4. Grid refinement. The characteristic number of nodes across the diameter and the total number of cells is displayed underneath each graph.

4. Numerical Validation

Based on the branching tube model chosen here, numerical grids are generated that extend 8 main tube radii downstream and upstream from the tube bifurcation of 120° and inlet to outlet diameter ratio of 1 ($L = 4$,$\alpha = 120°$, $r = 1$). The grid independence study is carried out for flow of Reynolds numbers $Re = 200, 400$

To estimate the error of the numerical computations and to ensure that numerical solution asymptotically converge to the physical solution, we solve for a number of successively finer geometries. The grid refinement is shown on Figure 4. The finest grid used is $N = 35$ and contains 1,213,167 cells.

Four different measures will be used for independence. The first measure uses the pressure drop between the inlet and the outlets. The second measure is the velocity profile at selected locations at the outlet. The third measure is the transfer function, i.e. the streamline mapping from the inlet to the outlet. And the final fourth measure is the distribution of the shear stress on the wall.

4.1. **Pressure Drop and Velocity Profile.** The pressure drop and the velocity profile are probably the easiest parameters to derive, but the least indicative of convergence. Convergence of these quantities is a necessary, but not a sufficient condition for grid independence since they are among the quantities that converge fastest and therefore other derived quantities of interest may not have converged yet. Nevertheless for completeness we present on Figure 5 the convergence for the pressure drop between the inlet and the outlets for successively finer grids.

Figure 6 give a comparison of the velocity profiles at selected locations of the outlet daughter tubes at N=25 and N=35.

4.2. **Transfer Function.** Streamlines are integrals of the velocity field and therefore it is expected that they will converge more slowly. Figure 7 illustrates the convergence of a single streamline.

To confirm grid independence the mixing patterns which are extensively studies in this paper, we need to confirm that the stream transfer function has converged. The stream transfer function is defined over the whole inlet cross-section, and hence to have an accurate measure for its convergence we need to take into consideration more than one streamline. For

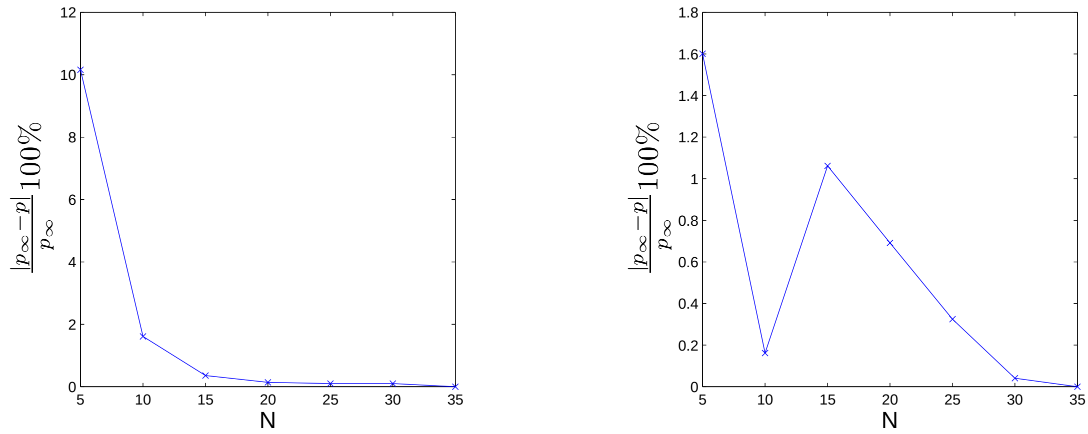

FIGURE 5. Pressure Drop.

this purpose we choose twelve evenly spaced points across the inlet (Figure 8) and integrate them along the velocity field until we reach the outlet. We use the following measure

$$\epsilon_N = \left(\frac{1}{n_S} \sum_{i=1}^{n_S} [T_N(\xi_i) - T_\infty(\xi_i)]^2 \right)^{\frac{1}{2}} \tag{29}$$

to quantify the expected average deviation of a streamline for a grid with a fineness of N. Here the index i runs over the streamlines, $n_s = 12$ is the total number of streamlines, and T_N and T_∞ are the transfer functions for a particular gird and the transfer function in the continuum limit. The continuum limit in our case is taken to be the grid with the finest mesh, i.e. $T_\infty = T_{35}$. The convergence of the result is shown on (Figure 9).

We can expect that for $N = 25$ the error in the stream transfer function to be around 2% of the diameter.

Later on we will apply the numerically obtained transfer function T_N repeatedly across successive bifurcations and we would be interested to know how the error propagates. The numerically obtained transfer function deviates from the analytical one.

$$[\chi_N, \beta_N] = T_N(\xi) = T(\xi) + \Delta T_N(\xi)$$

Here ξ_N describes the position on the outlet tube and β_N can have discrete values labeling the destination daughter tube.

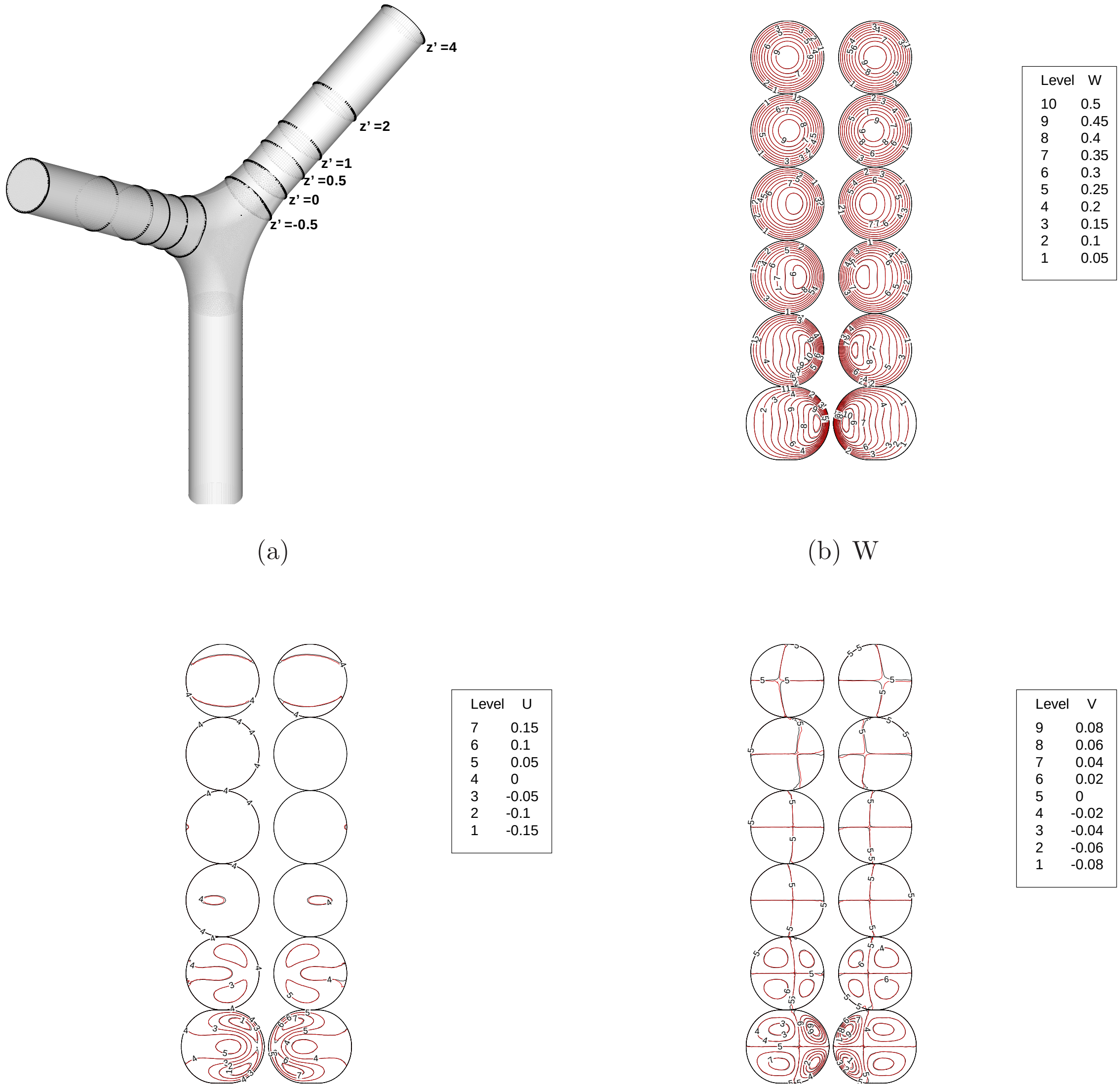

(a) (b) W

(c) U (d) V

FIGURE 6. Velocity contours for N=25(red) and N=35(black).

We expect that when $N \to \infty$ we will have $|\Delta T_N| \to 0$. The convergence will be smooth away from the symmetry plane orthogonal to the bifurcation plane, but it will have great oscillation close to that plane and on the plane the value of the function will be undefined since streamlines will terminate at the stagnation point of the internal bend of the bifurcation before reaching the outlet. Any variation around the plane will shift the stream from the one daughter tube to the other, thus causing a big error in the final output. This is the result of the fact that $\beta_N(\xi)$ is a step function and has a discontinuous first derivative.

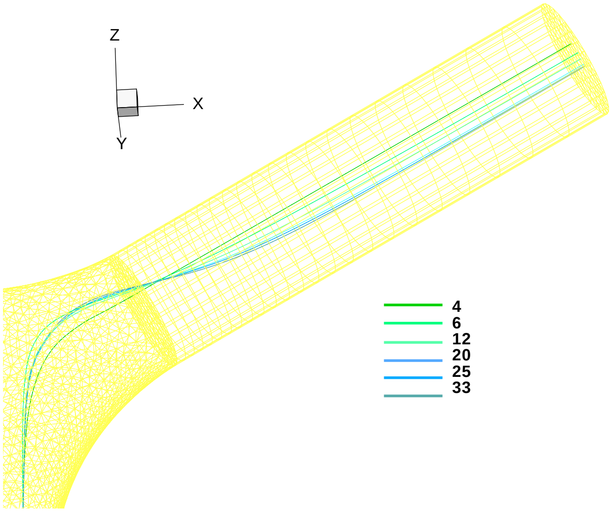

FIGURE 7. Convergence of a stream at $Re = 400$ starting at $\xi = (.25, .25)$

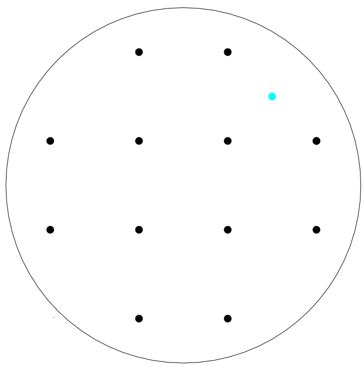

FIGURE 8.

Let us shift away from this region of discontinuity and consider regions that are not too close to the symmetry plane. Then

$$\begin{aligned} T_N^2(\xi) &= T^2(\xi) + T(T(\xi) + \Delta T_N(\xi)) + \Delta T_N(T(\xi) + \Delta T_N(\xi)) \\ &= T^2(\xi) + \frac{\partial T_N}{\partial \xi_i} \Delta T_{N,i}(\xi) + \Delta T_N(T_N(\xi)) + \mathcal{O}(\Delta T_N^2) \end{aligned}$$

where the subscript i denotes the spacial component. Clearly the propagation of the error will depend on the first derivative of the transfer function and the error can be expected to increase when the rate of mixing increases.

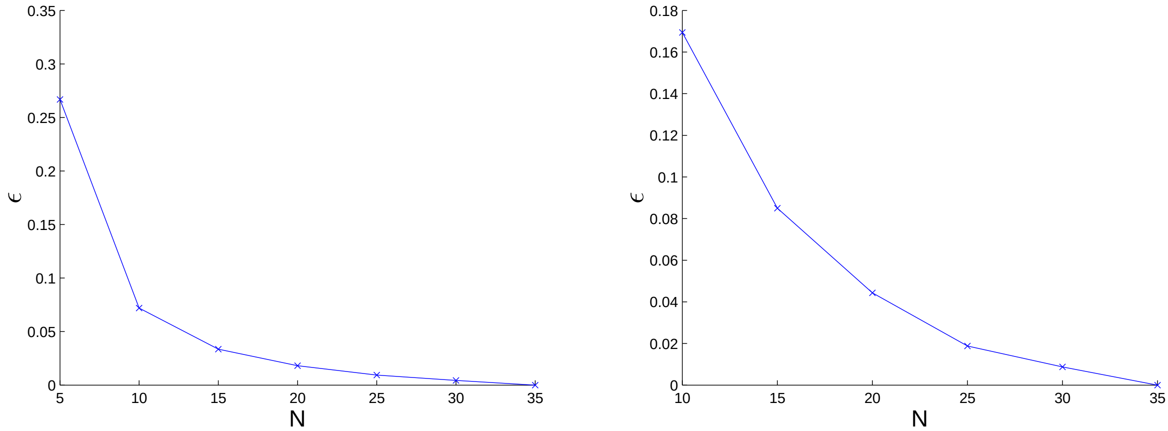

FIGURE 9.

4.3. **Normalized Wall Shear Stress.** The final measure of the numerical convergence of interest in this work is the distribution of the wall shear stress. The extracted values of the wall shear stress are normalized by the magnitude of the wall shear rate in a straight pipe with the same diameter, flow rate and Reynolds number.

As can be seen from Equation 15 the strain rate at the wall is dependent on the first derivative of the flow. Thus like the transfer function which is the integral of the velocity, the strain rate is another derived quantity and it will converge slowly. Figure 10 and 11 display the convergence of the wall shear stress for Reynolds numbers of 200 and 400 respectively.

The results are close, but there are some differences in the peak values especially in the case of the higher Reynolds number flow, where the grid may be insufficient to resolve some of the finer flow details. Nevertheless although coarse, the graphs are useful in giving a qualitative picture of the shear stress distribution.

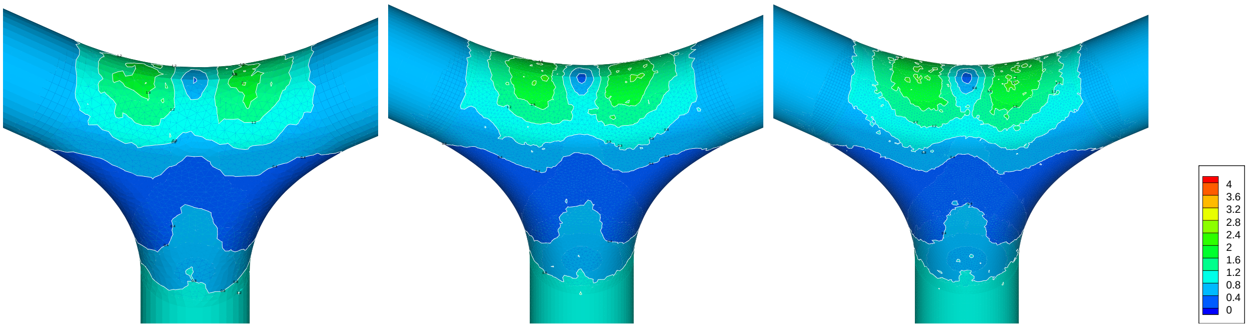

(a)

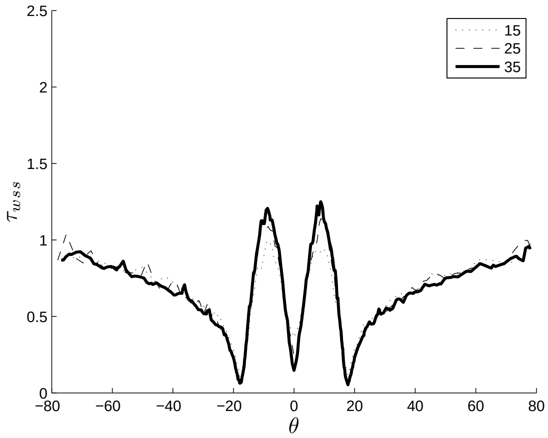

(b)

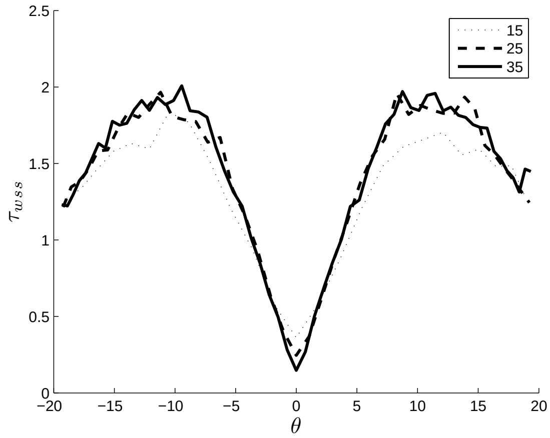

(c)

FIGURE 10. Wall Shear Stress for $N = 15, 25, 35$ and $Re = 200$ - top view (a), distribution along the top and bottom wall of the bifurcation (b), and along the internal wall of the bifurcation (c), θ being the deviation from the direction of the z-axis as viewed from the origin.

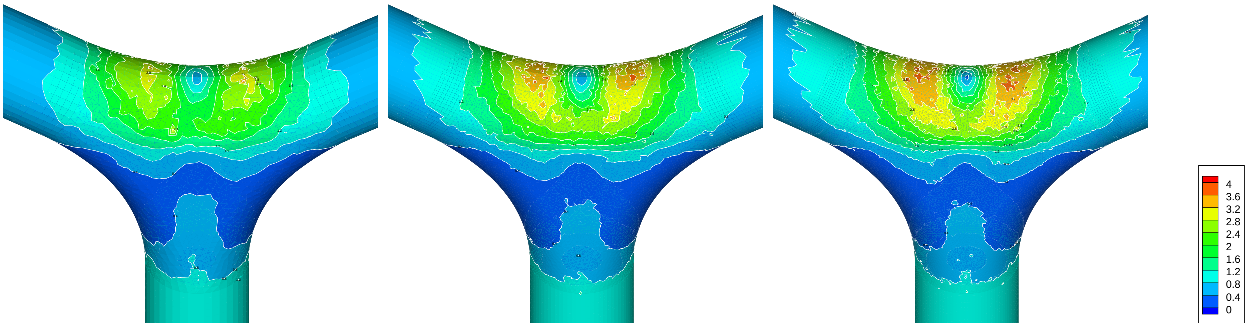

(a)

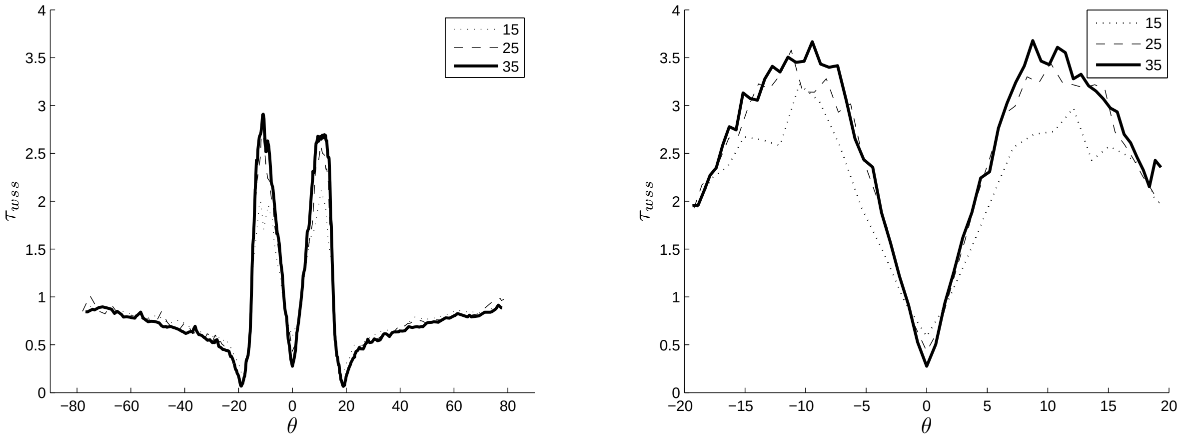

(b)

FIGURE 11. Wall Shear Stress for $N = 15, 25, 35$ and $Re = 400$. See caption of Figure 10. The contouring scale is the same.

5. Results and Discussion

Results are given for symmetrical flow with the following variations in parameter space $r = 0.5, 1$; $\alpha = 90, 120, 150, 180$; $Re = 200, 400, 600$.

5.1. **Flow Profile.** Profiles of the axial components of velocity along each daughter tube are depicted on Figure 12. The profiles consist of a sharp peak near the inner wall of the bifurcation which turns into a plateau towards the outer bend.

The emergence of the peak is caused by the centrifugal deflection of the faster moving central streams which displace the more slowly moving streams near the inner walls and thus also giving rise to a secondary velocity profile and a transverse pressure gradient. The emergence of this sharp peak near the inner wall leads to a high velocity gradient and a high shear stress on the wall. Likewise the plateau-like velocity profile in the inner bend with almost a zero gradient leads to a very small shear stress on the outer side of the wall. The shear stress will be discussed exclusively in a later subsection.

Comparing the results for different Reynolds numbers we note that a correlation exists between how high the Reynolds number is and how sharp the observed peak is. In the bifurcation region the profiles for different Reynolds numbers do not differ much but further downstream the difference starts to become increasingly pronounced.

Downstream from the bifurcation the low Reynolds number flow becomes fully developed quite early at a distance of around 2D from the entrance of the daughter pipe, whereas the high Reynolds number flow of around $Re = 600$ takes much longer to obtain its developed parabolic profile.

In addition to the 2D plots along the bifurcation plane, a three dimensional plot of the velocity profile is presented on Figure 13 for a flow with a Reynolds number of 400. The axial velocity emerges from the bifurcation with the shape of a sofa with a crest which peaks close to the inner wall of the bifurcation and descends slowly in the tangential direction, but goes down very steeply in the radial direction. Further downstream the crest engulfs the central depression. At the distance of $L = 4D$ the flow seems to have restored its parabolic profile and looks more like a volcano.

Given the wide range of bifurcations in nature it may also be of interest to study how the velocity profile is affected by varying the angle. Tadjfar [13] has considered only bifurcation

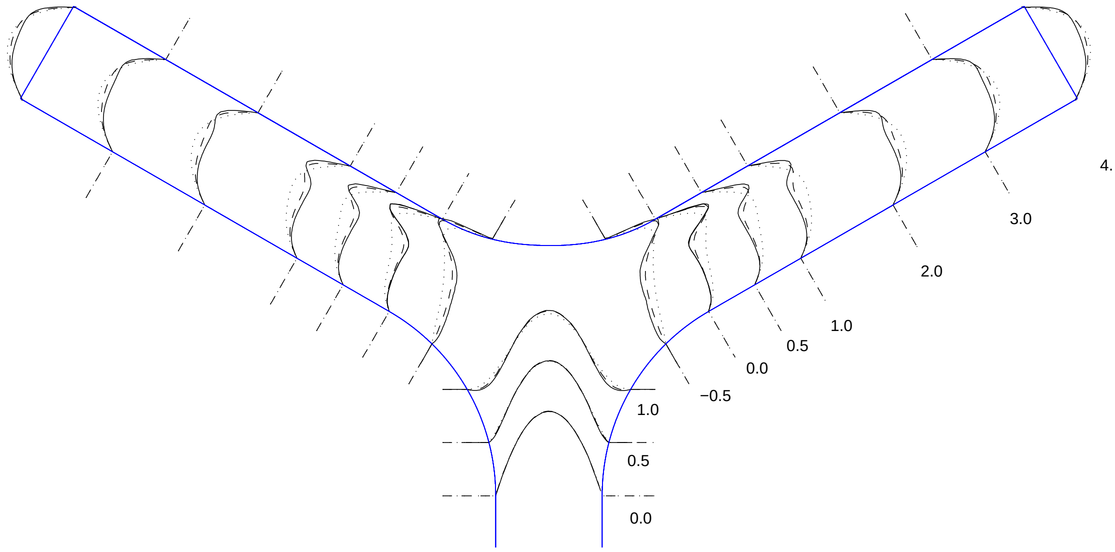

FIGURE 12. Axial velocity profile for Reynolds numbers of 200 (dotted), 400 (dashed) and 600 (solid). The distance is measured in units of the diameter.

angles that are less than 90°. We extend his work by considering obtuse bifurcation angles. Figure 14 illustrates the profile at the entrance to the straight section of the daughter tube for angles ranging between 90° to 120°. Greater deflection angles as expected lead to higher centrifugal forces, result in a more steep peak this also giving rise to a higher shear stress on the wall (due to the higher velocity gradient).

To understand the flow fully it is necessary to consider the transverse velocity and pressure gradients in addition to those in the acial axial direction. Figure 15 shows the secondary velocity for three values of the Reynolds number. Unlike the case of a confluence [7] where one observes 4 vortices, in the case of a bifurcation there are only two. It should be noted that the strength of the secondary flow is positively correlated with the Reynolds number, and in general does not exceed 10% of the maximal axial velocity. Downstream the strength of the vortices is gradually dissipated by the action of viscosity. The effect of the vortices is that within each daughter tube the fluid particles flow in two spiraling coils that are of opposite helicity and do not mix with each other.

Dependence of the secondary velocity field for different bifurcation angles α is also presented on Figure 16. Increasing the angle of bifurcation leads to higher secondary velocity.

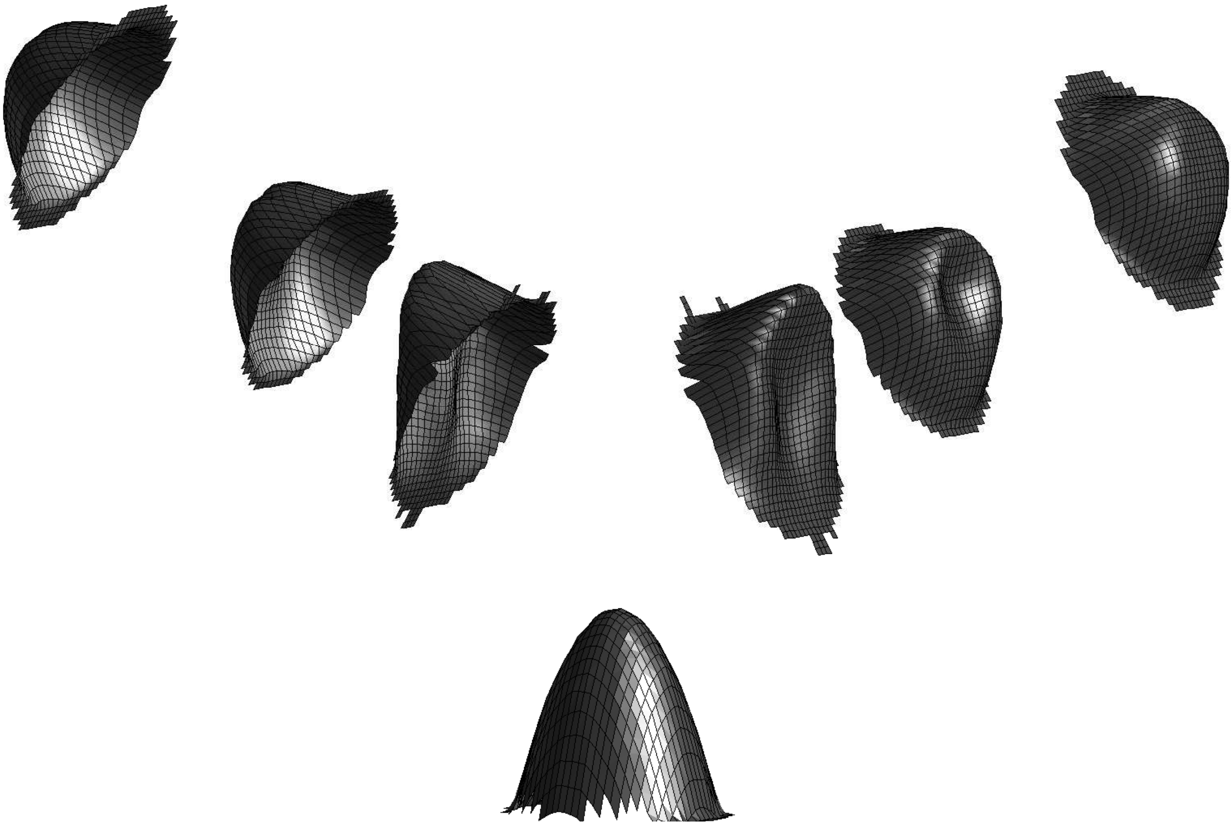

FIGURE 13. Axal velocity profile for a 120° bifurcation and $Re = 400$

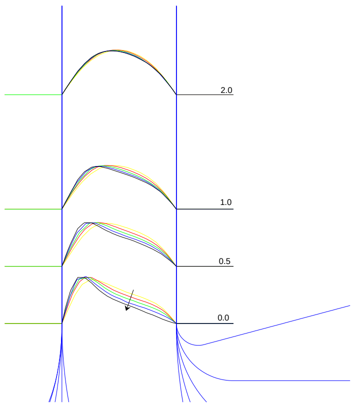

FIGURE 14. The axial velocity profile at the right daughter tube for bifurcation angles of 90°(yellow), 120°(red),150°(green),180°(blue),210°(black) and a Reynolds number of 200. Arrow indicates increasing angle.

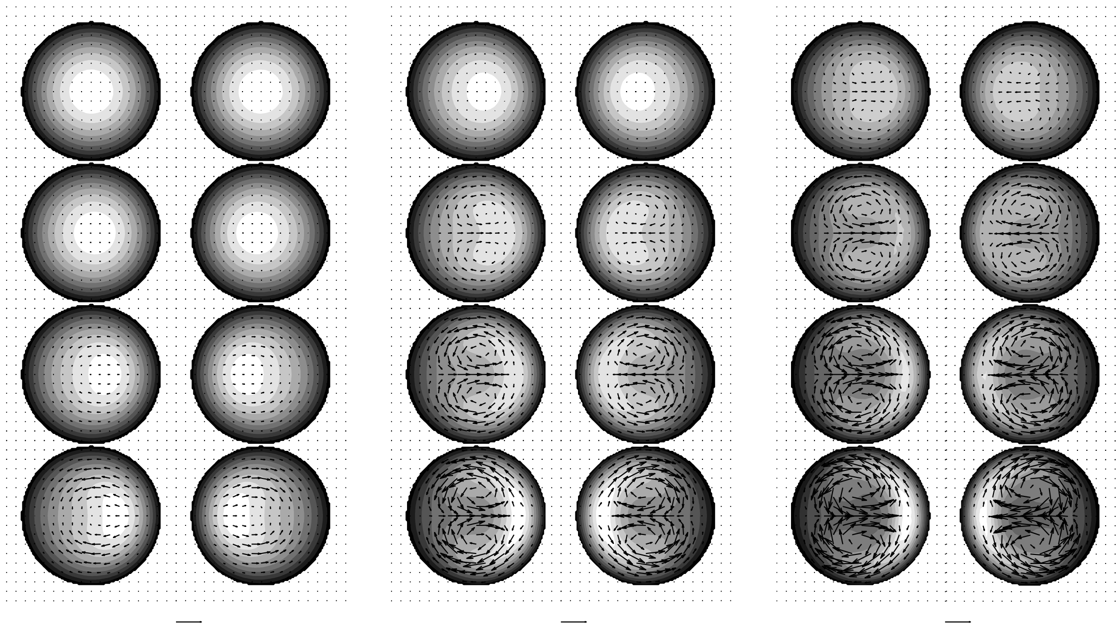

Figure 15. Variation of transverse velocity with Re for values of 200,400 and 600 at several downstream stations (0.5D, 1D, 2D, 4D). The arrow underneath each graph represents 1/10 of the axial velocity. Contours of the axial velocity are also presented.

For completeness pressure is also presented on Figure 17. The pressure distribution is mostly dictated by the local geometry of the tubes. It is linear within the pipes and as noted by Tadjfar [13] too the effect of the bifurcation is limited to no more than $2D$ from the bifurcation.

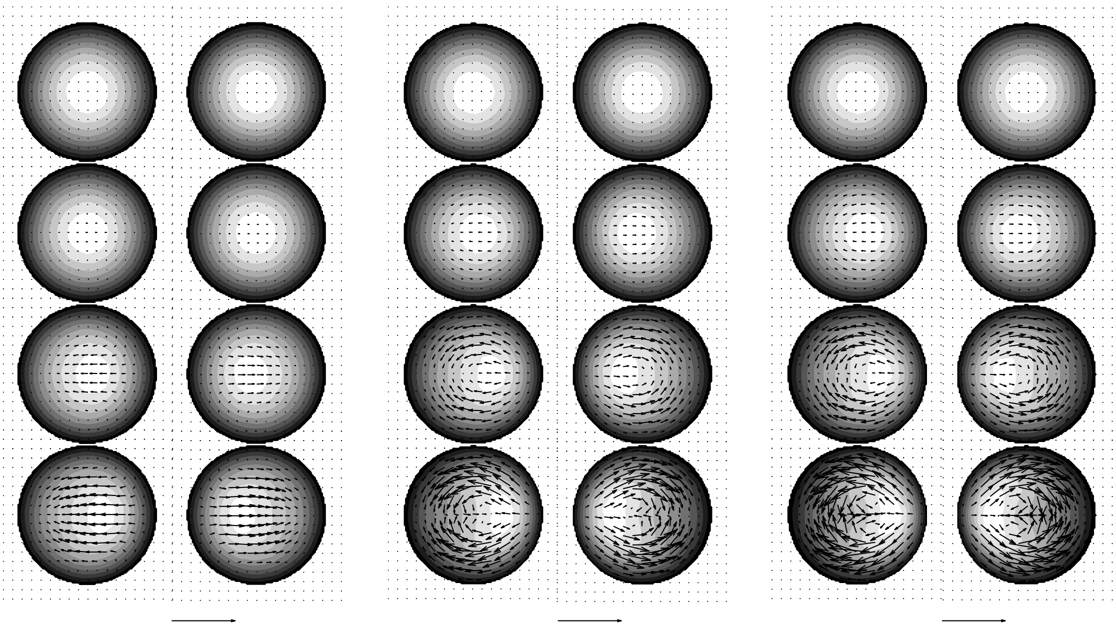

FIGURE 16. Variation with $\alpha = 90, 150, 180$. The arrow represents 1/10 of the maximal velocity along the mother tube.

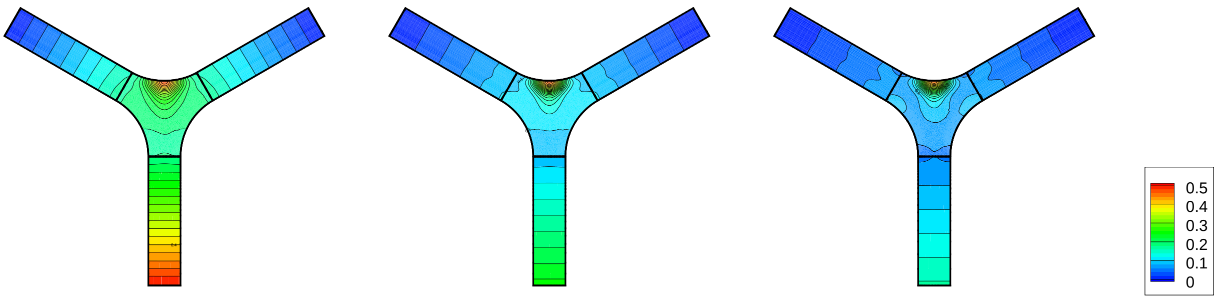

FIGURE 17. Re=200,400,600 pressure field

5.2. **Advective Mixing.** If there were no bifurcation the streamlines would remain straight lines, and the stream transfer function would be the identity. The bifurcation introduces dispersion of the streamlines and shifts the stream transfer function away from the identity as can be computed by the method described in Section 2.4.

It is of interest to study what the trajectories of particles in a bifurcating flow would be. Computing the transfer function would allow us to compute the mixing patterns for situations where the dominant dispersion mechanism for the solute particles is advection, and all effects of molecular diffusion and the inertia of the particles can be neglected. Only then would the particle trajectories coincide with the streamlines (the steady flow requirement for this is also met).

To illustrate the mixing we color-code the fluid with different color at the inlet and we observe how the color is distributed at the outlet.

One concern with the numerical method of calculating the mixing pattern is whether the results are dependent on the length of the inlet and outlet tubes. Figure 18 compares the mixing pattern for L=4 and L=8 and as can be seen no differences between the color pattern at the two different stations can be visible meaning that the pattern has reached its final asymptotic distribution.

Mixing patterns will be considered for varying Reynolds numbers.

Figure 19 illustrates the mapping of streamlines from the input to the two outputs of a bifurcating pipe at different Reynolds numbers for a geometry with $r = 1$ and $\alpha = 120°$.

The imperfections of the numerical method are evident by the white spaces close to the boundary. In theory all streamlines must reach and terminate at the outlet as required by the continuity equation, in practice due to the finitely many integration steps that can be performed on a modern computer, the streamlines close to the boundaries where the velocity is close to zero never really reach the outlet. In addition due to the finite grid size some of the streamlines get deflected away from the computational domain and can be terminated prematurely.

To visualize the results three coloring patterns have been used - radial, left-to-right and top-to-bottom. From Figure 19 it is evident that the mixing pattern is richer for higher Reynolds numbers and the spiraling/coiling motion is clearly visible.

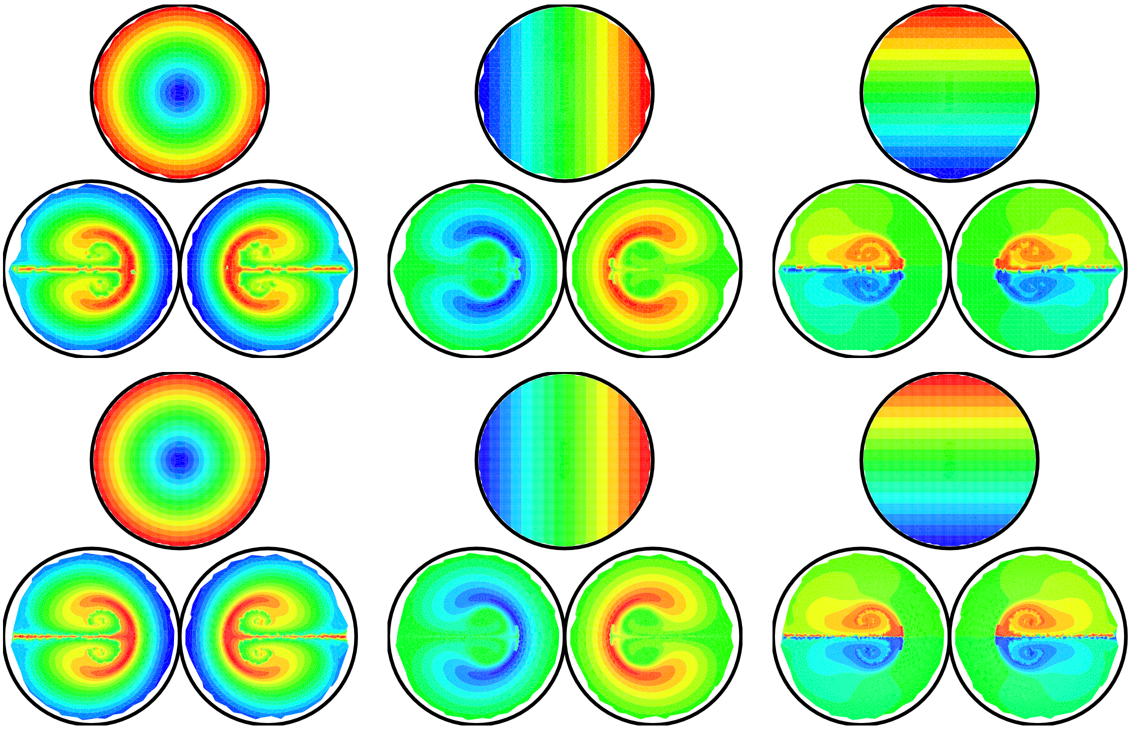

FIGURE 18. Mixing $L = 4$ and $L = 8$ at $\alpha = 120°$, $r = 1.0$ and $Re = 120°$. The two results are almost identical confirming that the at L=4 the mixing has reached its asymptotic value

It is important to note that as expected the top-bottom and left-right symmetries of Equation 14 are manifest in the mixing patterns.

Of particular interest is the mixing of the fluid which is color-coded radially since it illustrates the mixing of the boundary layer. At the outlet the boundary layer (red) in the mother tube is injected towards the centers of the daughter tube, and while for Re=200 the injection is only partial since some of the red painted fluid is still in contact with the wall, for higher Reynolds numbers the boundary layer is completely shifted into the center and obtains a coiled shape. Likewise the central layers of the mother tube are distributed along the boundaries of the daughter tubes, and the higher the Reynolds number the more even the distribution is.

This mixing pattern indicates that bifurcations may play an important role in the exchange between the vessel walls and the delivering fluid within. Since most of the exchange occurs at the boundary, we would expect that the boundary layer will be mostly depleted before the

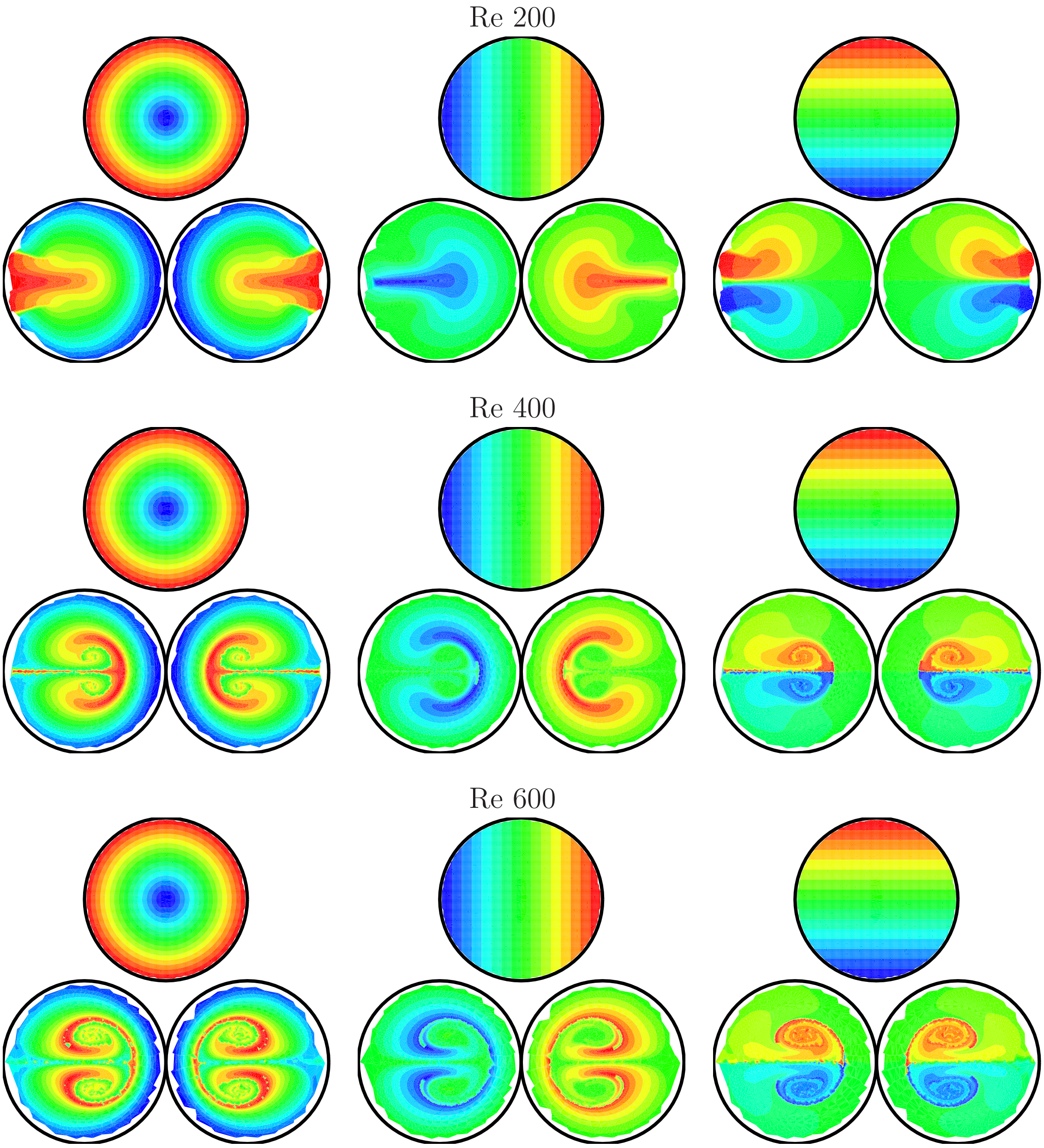

FIGURE 19. Mixing

bifurcation, but after the bifurcation the richer central part of the fluid will spread towards the periphery thus replenishing the vessel walls.

5.3. **Recursive Advective Mixing.** To compute the mixing along several generations of bifurcations the direct method would be to rerun the numerical simulation for the new geometry. But this is impractical for a large number of bifurcations given the complexity of the geometry and the large amount of computational time necessary to obtain meaningful results. To avoid the laborious numerical computations we take a shortcut by assuming that the distances between each generation of bifurcations are great enough that any downstream and upstream influence among them is negligible. Then it would be simply a matter of applying the stream transfer function repeatedly in order to obtain the mixing pattern after each generation of bifurcation.

This of course is a simple model, which is quite detached from realistic bifurcations within the human body, where the growing boundary layer after the bifurcation will not generally become comparable to the radius of the daughter tube, and thus the next bifurcation will disturb the flow before it has had a chance to reach its fully developed state, and a new modified boundary layer will be formed. In such cases an exact numerical simulation is indispensable. Nonetheless considering this simple model may still give important insights into more complicated models.

In order to avoid recomputing the transfer function at each bifurcation, we choose the mother-daughter tube diameter ratio so that the Reynolds number in each successive generation of bifurcations is constant. At each branching we have $D \to D/r$ and by the incompressibility requirement $v \to vr^2/2$ To ensure that the Reynolds number remains the same we require

$$Re = \frac{\rho v D}{\mu} = \frac{\rho \frac{vr^2}{2} \frac{D}{r}}{\mu} \to r = \frac{1}{2} \tag{30}$$

meaning that the diameter of the daughter tube is half that of the mother tube, meaning that at each generation the total outlet area decreases by half, and the velocity increases by a factor of two. This assumption is necessary to save the computational time of recomputing the transfer function for the different Reynolds numbers at each generation, but it is unfortunately an unrealistic one since for physiologically relevant flows such as the rapidly branching network of the airways the cross-section at each generation increases, while the radius of each daughter tube decreases [6].

Figure 20 illustrates the network of successive bifurcations (to 4th generation) that is the next item we will consider next. The top row consists of coplanar bifurcations, and the bottom row of out-of-pane bifurcations.

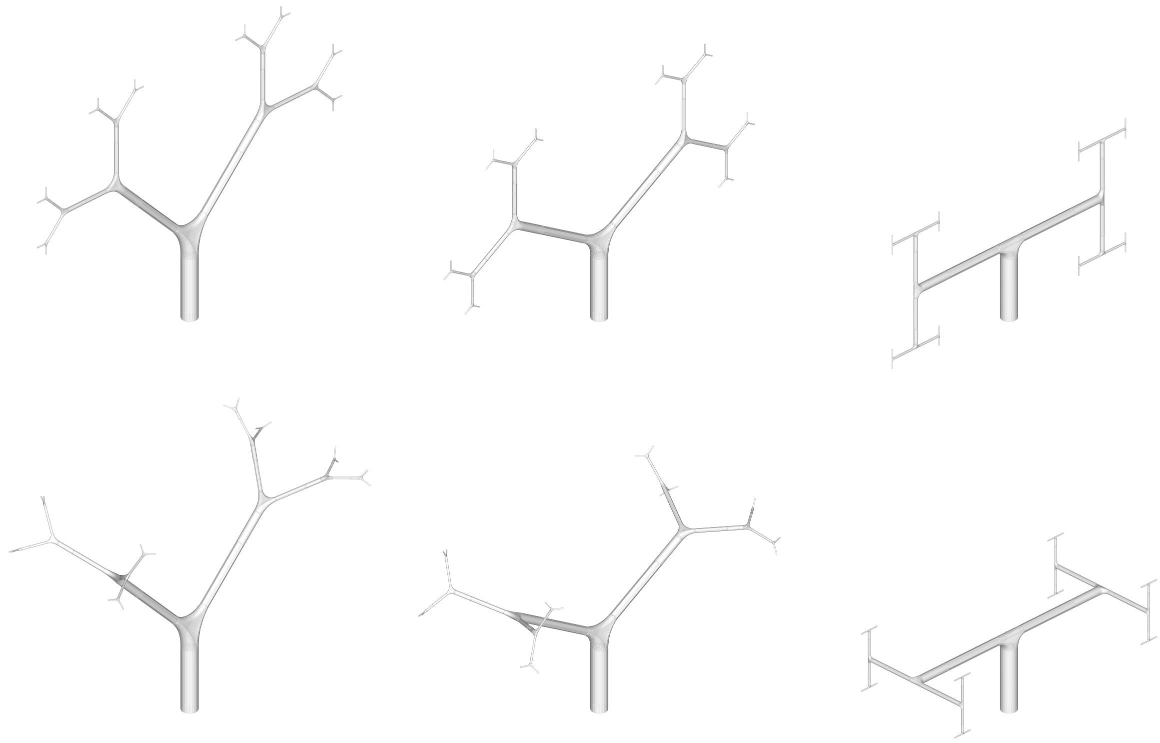

Figure 20. Multiple successive bifurcations of $\alpha = 90°, 120°, 180°$ (left to right) for planar and out-of-plane arrangements (top to bottom)

Figures 21, 22 and 23 illustrate the mixing patterns for $r = 1/2$ for Reynolds numbers of 200 and 400, and bifurcation angles of 90°, 120°, 150° and 180° respectively for the planar geometry. The coloring at each station is subjected to repetitive stretching and folding, which is more extreme at higher angles and Reynolds numbers. The evolution of the central stream tube (colored in black) is to be considered. For the planar geometries of Figures 21 - 23 it is evident that at each station the central region is spread towards the periphery, and the peripheral region is condensed towards the center. Thus the bifurcation plays an important role of "switching" the center and the boundary which certainly makes the exchange of materials between the fluid and walls of the vessel more efficient.

Figures 24, 25 and 26 illustrate the mixing patterns in the case of the out-of-plane geometry.

The figures are included for reference for future experiments studying the advective mixing in a bifurcation.

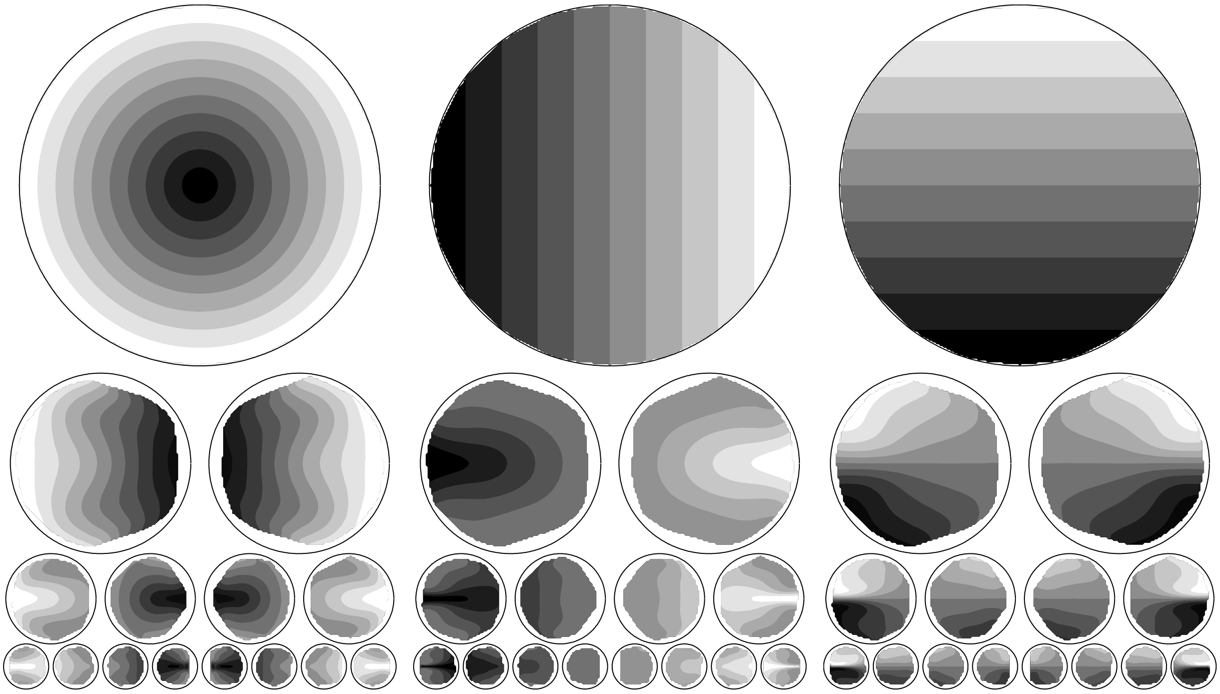

(a) $Re = 200$

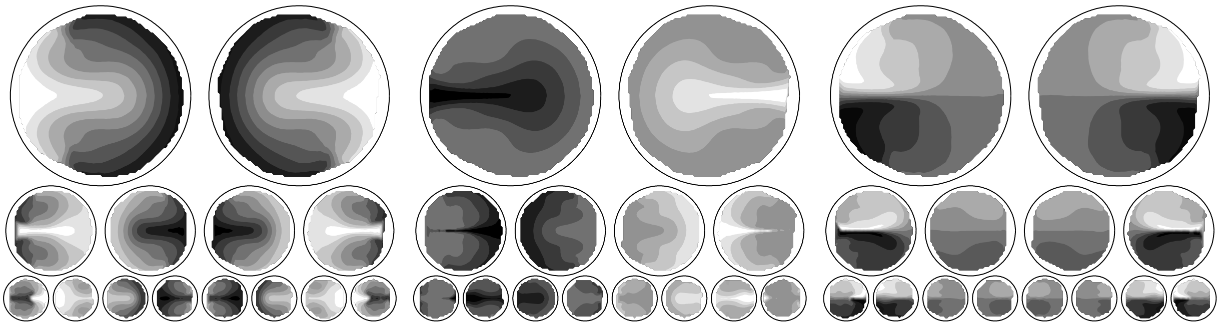

(b) $Re = 400$

FIGURE 21. Planar Geometry $\alpha = 90°$

It should be noted that the system is still invariant under both symmetries noted in Equation 14, and that those symmetries are manifest in the results.

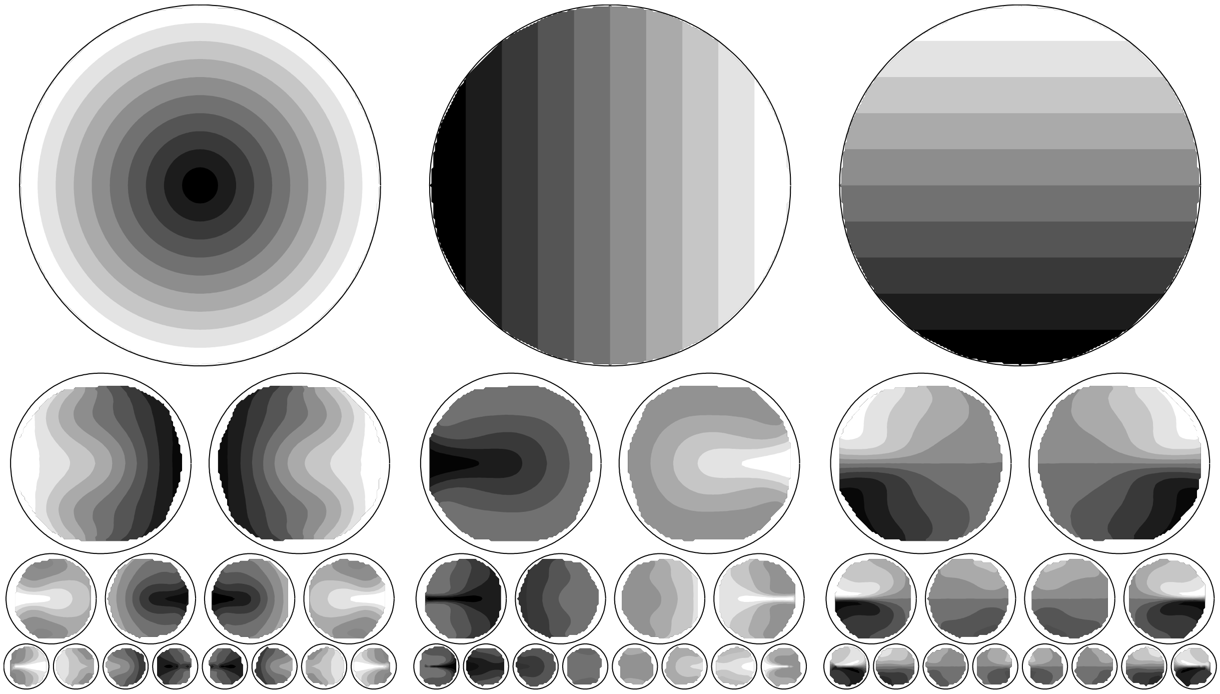

(a) $Re = 200$

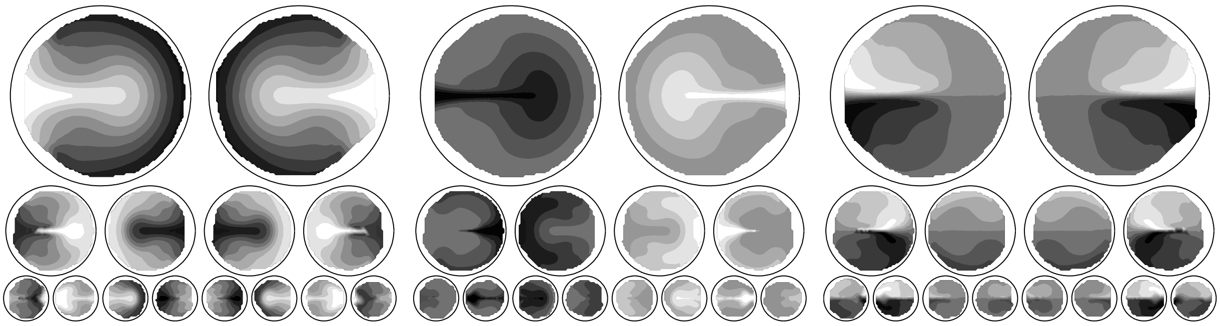

(b) $Re = 400$

FIGURE 22. Planar Geometry $\alpha = 120°$

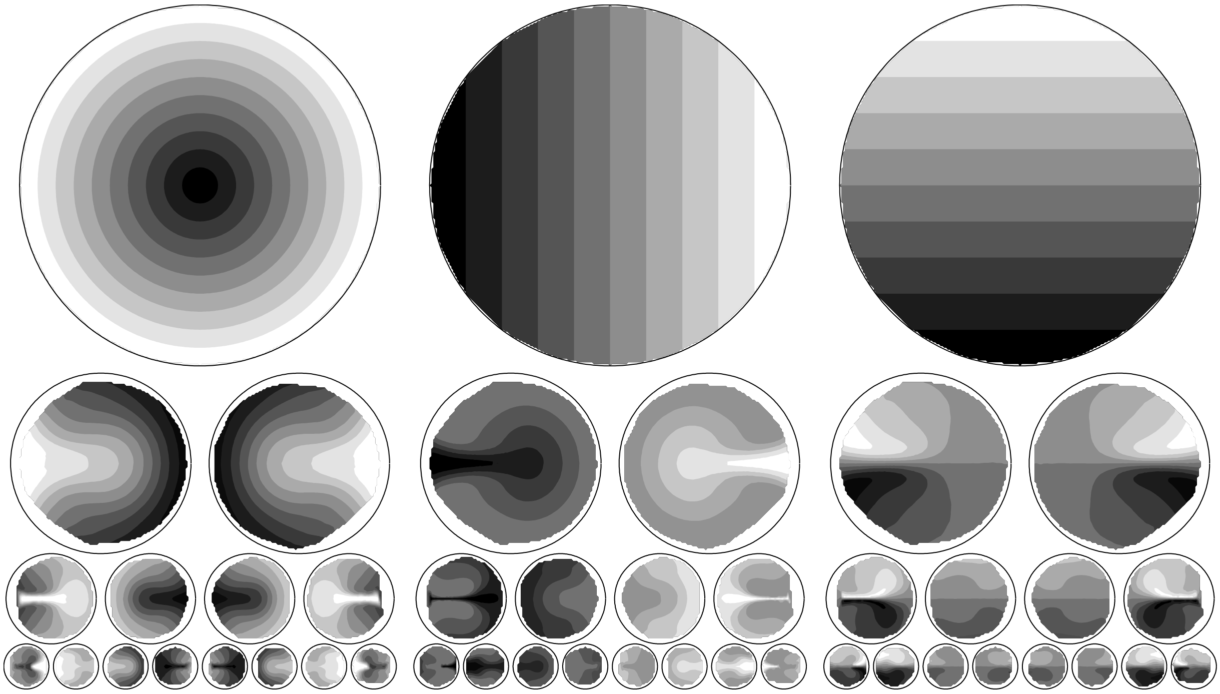

(a) $Re = 200$

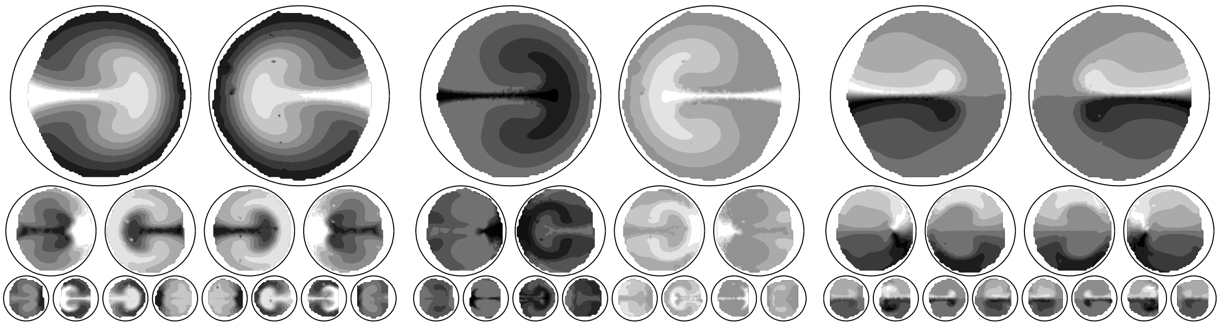

(b) $Re = 400$

FIGURE 23. Planar Geometry $\alpha = 180°$

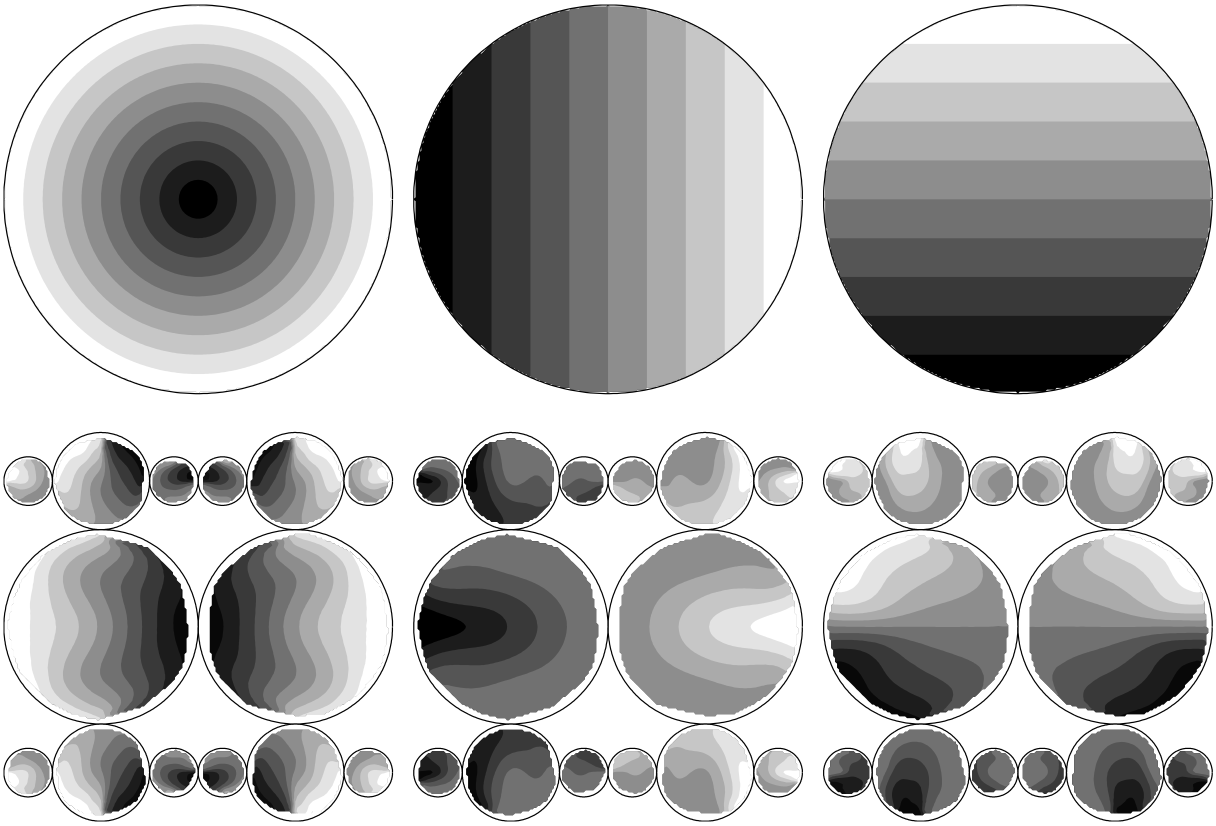

(a) $Re = 200$

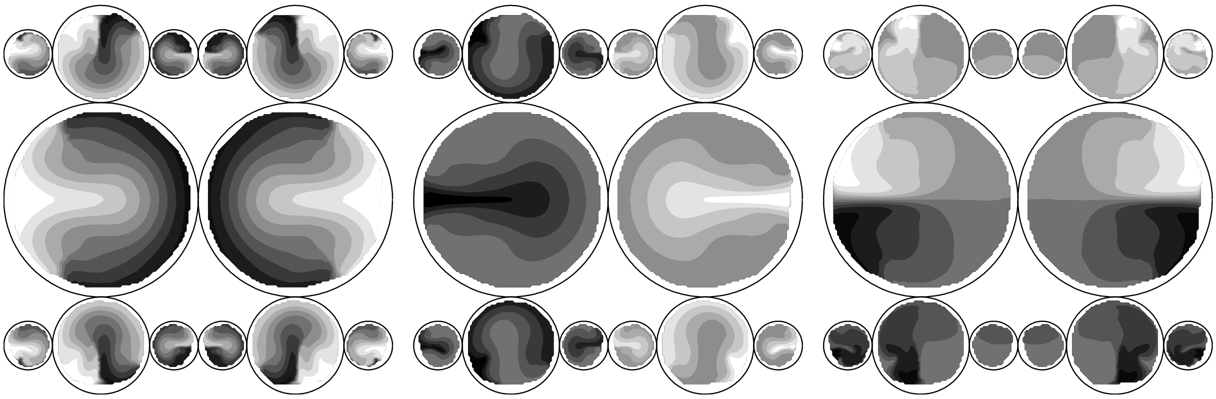

(b) $Re = 400$

FIGURE 24. Out-of-Plane Geometry $\alpha = 90°$

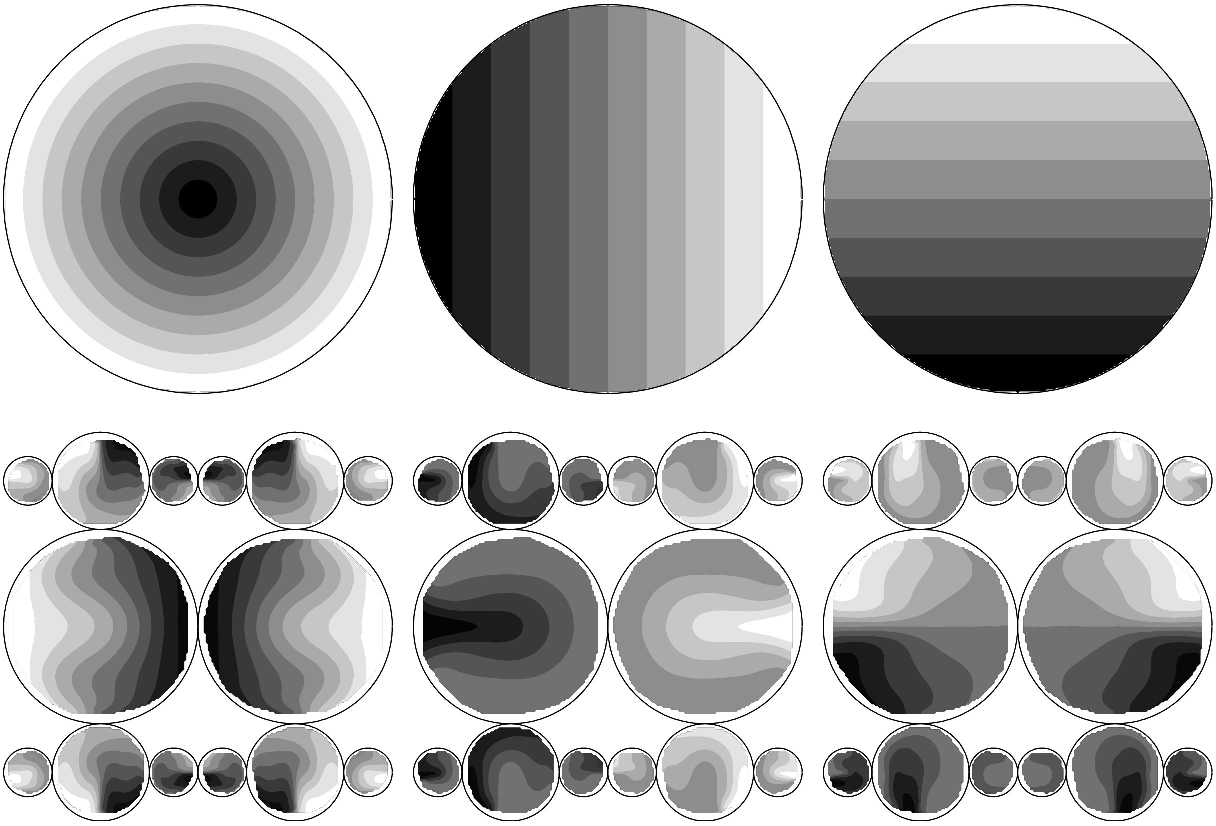

(a) $Re = 200$

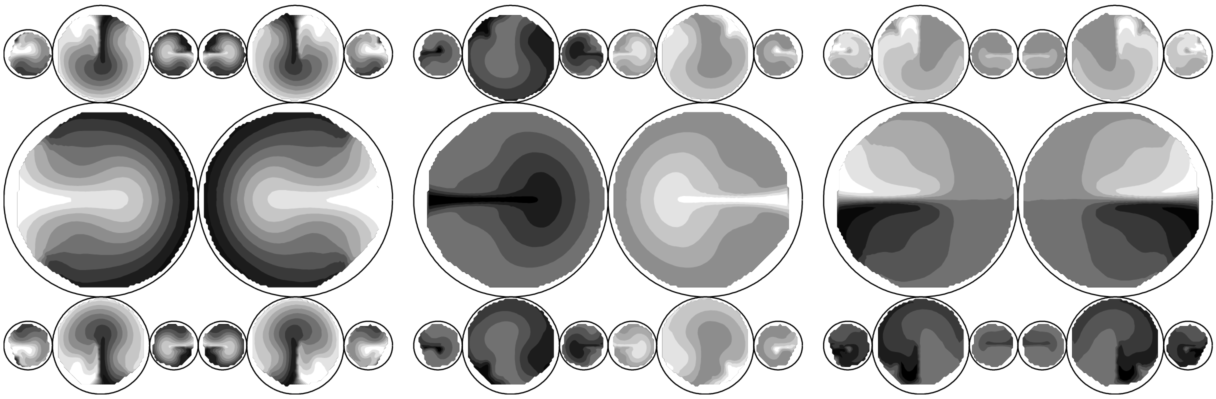

(b) $Re = 400$

FIGURE 25. Out-of-Plane Geometry $\alpha = 120°$

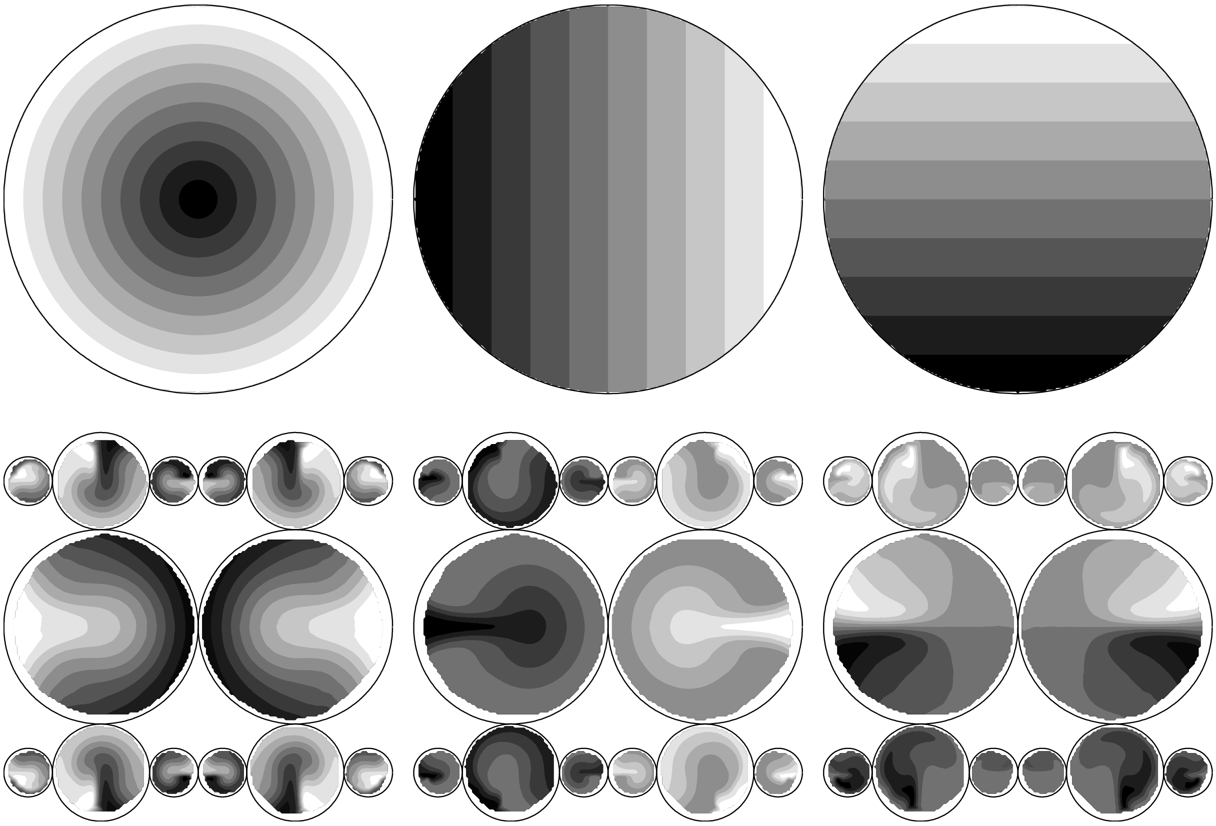

(a) $Re = 200$

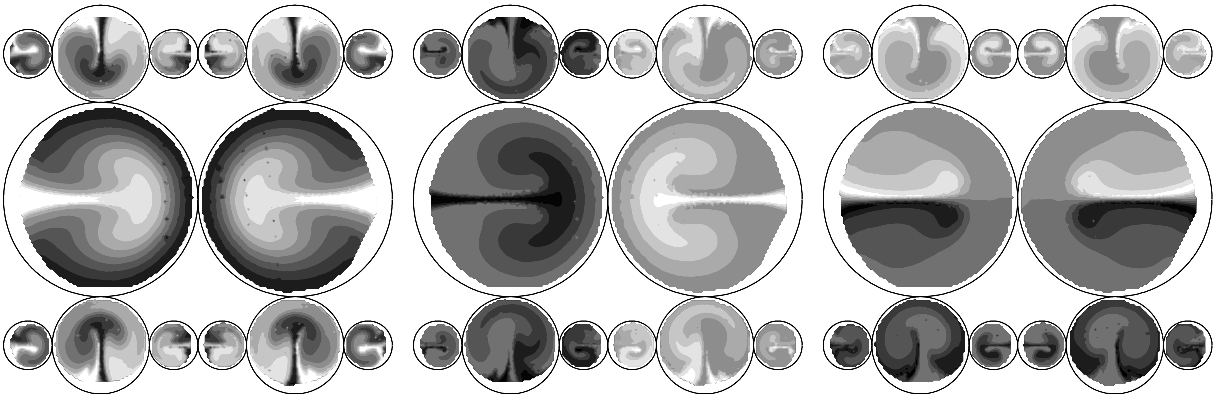

(b) $Re = 400$

FIGURE 26. Out-of-Plane Geometry $\alpha = 180°$

5.4. **Wall Shear Stress.** It is hypothesized that wall shear stress sites within are often the sites of high risk of vascular diseases and atherosclerosis [13, 4]. Preferential sites include the outer walls of the daughter tubes and inner wall of the bifurcation as will also be confirmed by this study.

The wall shear stress is shown for several different angles for $r = 0.5$ and $r = 1.0$. The extracted values of the wall-shear stress are normalized by the magnitude of the wall shear rate in a straight pipe with the same diameter, flow-rate and Reynolds number.

The areas of low shear stress are readily identifiable from these figures and using the empirically established negative correlation between intimal thickening and shear stress, one can deduce that the areas most vulnerable to atherosclerosis are the outer walls at the bifurcations, and the central part of the splitting wall.

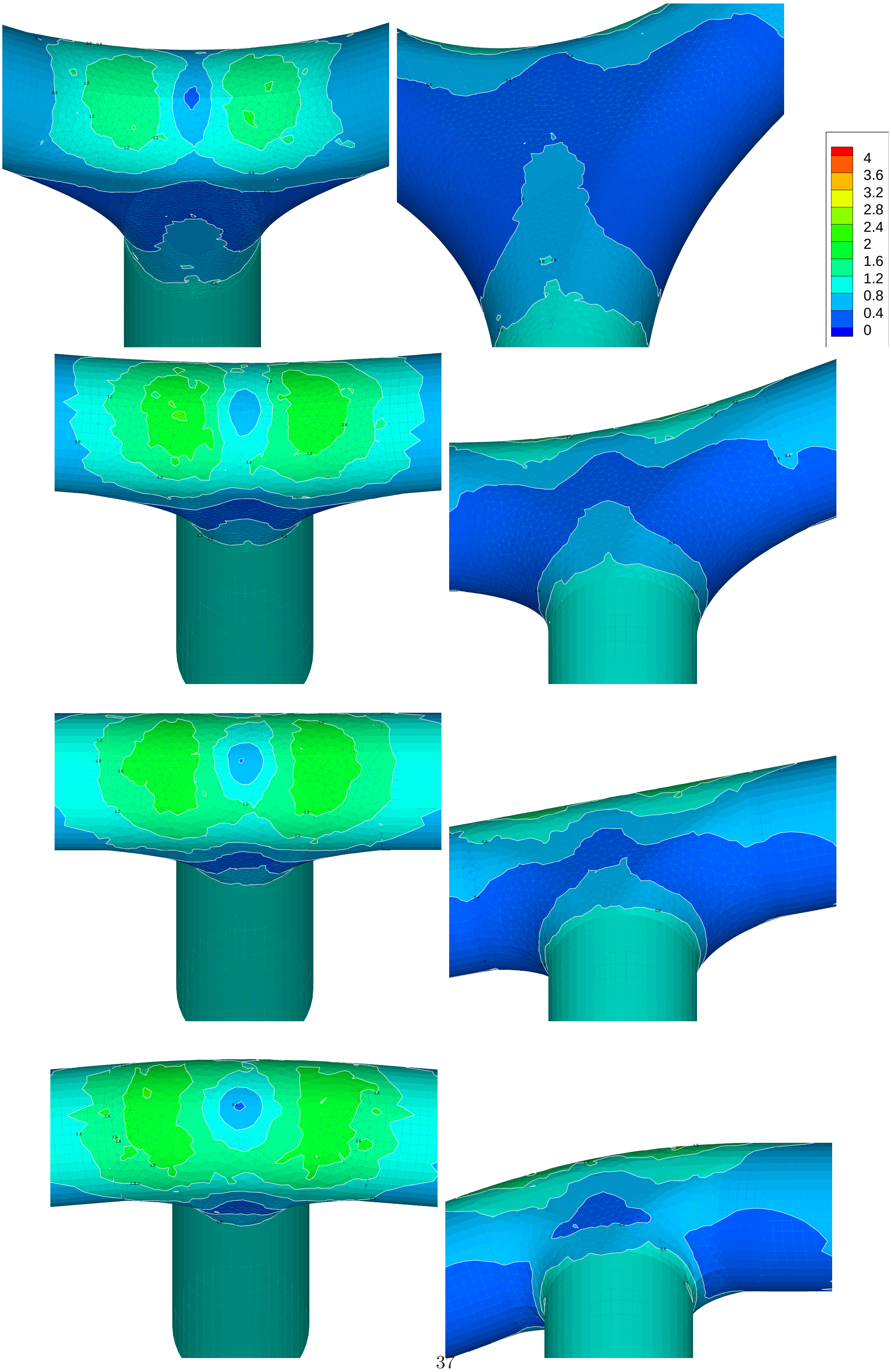

FIGURE 27. Wall Shear stress for $r = 1.0$ and $\alpha = 90, 150, 180, 210$

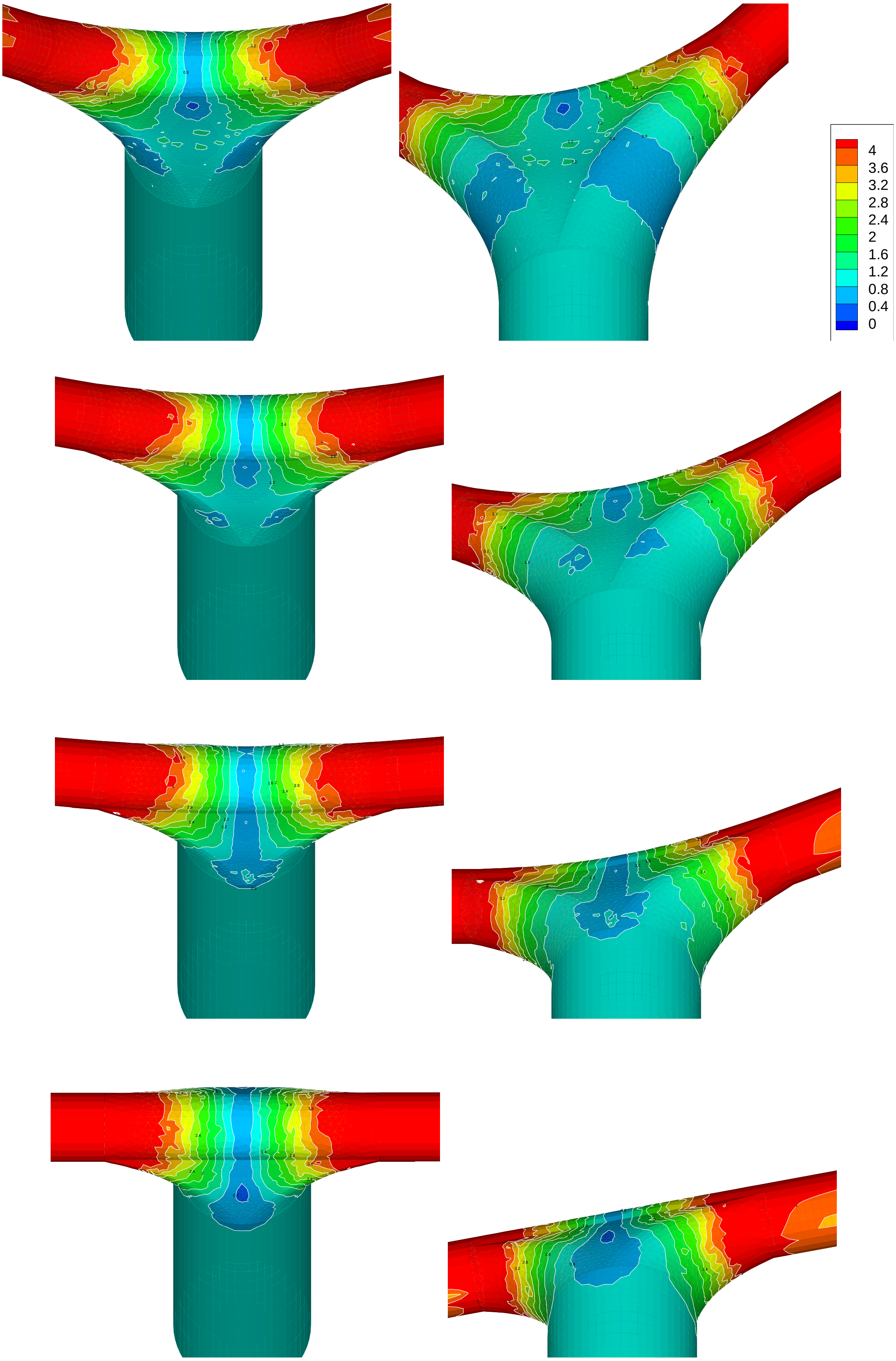

FIGURE 28. Wall Shear stress for $r = 1.0$ and $\alpha = 90, 120, 150, 180$

6. Conclusion

We have studied the velocity-field, shear-stress distribution and the advective mixing for a single and a repeatedly branching system of tubes over a range of Reynolds numbers, diameter ratios and bifurcation angles. We have obtained numerically accurate results, confirmed by extensive grid-independence studies.

A number of simplifying assumptions have been made in this study including (i) rigid walls, (ii) Newtonian fluid and (iii) steady flow. The vessel elasticity and deformation is a factor which will mostly affect the flow close to the vessel boundaries and its effect on the mixing will be minimal, although it might cause more significant variations in the shear stress distribution. The Newtonian approximation for the fluid is also a valid one especially so when one considers the blood in larger arteries and the air in the lungs since size of the fluid particles is negligible. Of course for capillaries where the diameter becomes comparable to the size of the red blood vessels the rheological characteristics of blood will become more pronounced and the newtonian approximation will fail.

The assumption of steady flow does have some serious drawbacks since significant effects of flow acceleration and deceleration are ignored. Yet, this study is only concerned with capturing the effect of the local geometry, and in a future paper the effect of the unsteadiness may be added into consideration.

The mixing patterns derived show that each bifurcation acts as a switcher between the richer central stream tube and the boundary streams, thus replenishing the wall boundaries with the richer fluid in the center.

The wall-shear stress distribution found in this study agrees with previous such studies and confirms clinical results that the most vulnerable sites to atherosclerosis are the outer walls of the dividing arteries and the inside walls of the bends, which are characterized by a low shear stress.

FIGURE 29. Once and twice-curved pipes

APPENDIX A. MIXING IN CURVED PIPE

Murata, Miyaka and Mirane [5] compute the flow in a once-, twice-curved pipe . We will take their results to obtain an analytical result for Stream Transfer function to first order in the small parameter κ describing the curvature. We will only consider the once- and twice-curved cases. The geometry of the pipes in these two types of flows will be determined by the center-line equations

$$\hat{y} = (1 + \kappa^2 \hat{z}^2)^{\frac{1}{2}} \tag{31}$$

$$\hat{y} = \tanh(\kappa \hat{z}) \tag{32}$$

which describe once- and twice-curved cases respectively.

By expanding the solution for the flow in the small parameter κ

$$v = v_0 + \sum \kappa^{n+1} v_n \tag{33}$$

where v_0 is the Poiseuille flow

$$v_0 = \begin{bmatrix} 0 \\ 0 \\ 1 - r^2 \end{bmatrix} \tag{34}$$

And the first order correction is given by

$$v_1 = \begin{bmatrix} -\frac{Re}{288}(1-r^2)^2((4-r^2)\cos\theta\frac{1}{\kappa^2}\frac{d^2y}{dz^2} \\ \frac{Re}{288}(1-r^2)((4-23r^2+7r^4)\sin\theta\frac{1}{\kappa^2}\frac{d^2y}{dz^2} \\ -r(1-r^2)\left(\frac{Re^2}{11520}(19-21r^2+9r^4-r^6)-\frac{3}{4}\right)\cos\theta\frac{1}{\kappa^2}\frac{d^2y}{dz^2} \end{bmatrix} \tag{35}$$

$$v = v_0 + \kappa^2 v_1 + \mathcal{O}(\kappa^3) \tag{36}$$

$$\sigma_0(t) = x_0 + tv_0 \tag{37}$$

Applying Equation 18 successively to σ_0 we obtain that to order κ^2 it converges on the second iteration

(38)

$$\begin{aligned} &\sigma_3(t) \\ &= \sigma_2(t) + \mathcal{O}(\kappa^3) \\ &= \begin{bmatrix} r_0 \\ \theta_0 \\ z_0 + (1-r_0^2)t \end{bmatrix} \\ &+ K \begin{bmatrix} -Re(1-r_0^2)^2(4-r_0^2)\cos\theta_0\ t \\ Re(1-r_0^2)(4-23r_0^2+7r_0^4)\sin\theta_0\ t \\ \frac{r_0}{40}(1-r_0^2)\left[-8640+Re^2(19-21r_0^2+9r_0^4-r_0^6)-40Re(4-5r_0^2+r_0^4)\cos\theta_0\ t\right] \end{bmatrix}\kappa^2 \\ &+ \mathcal{O}(\kappa^3) \end{aligned}$$

$$K = \begin{cases} \frac{1}{128} & \text{onces-cruved case} \\ \frac{e^2(e^2-1)}{36(1+e^2)^3} \approx \frac{1}{18378} & \text{twice-cruved case} \end{cases} \tag{39}$$

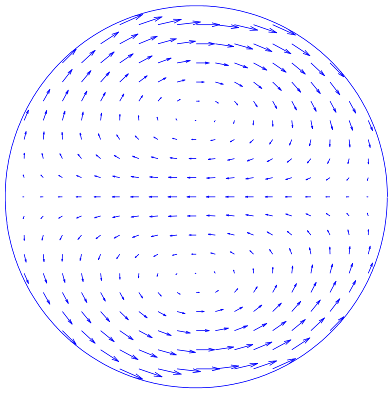

FIGURE 30. Infinitesimal mixing pattern for a curved pipe. The mixing in the center is from the inner towards the outer wall of the bend.

$$\xi_1 = r_0 \qquad \xi_2 = \theta_0$$

$$\chi_1 = r_1 \qquad \chi_2 = \theta_1$$

$$t = \frac{z_1 - z_0}{1 - r_0^2} + (O)(\kappa^2) \tag{40}$$

Hence the transfer function from z_0 to z_1 will be

$$T_{z_0 \to z_1}(\xi) = \xi + KRe(z_1 - z_0) \begin{bmatrix} -(1-\xi_1^2)(4-\xi_1^2)\cos\xi_2 \\ (4 - 23\xi_1^2 + 7\xi_1^4)\sin\xi_2 \end{bmatrix} \kappa^2 + \mathcal{O}(\kappa^3) \tag{41}$$

Usually we would be interested in $T_{-\infty \to +\infty}$ but unfortunately this expansion method is not appropriate since as can be seen from Equation 41 it would give an infinite result for finite κ. In order to be able to obtain a meaningful result we need to consider the expansion of the transfer function to all orders of κ which is very difficult to do analytically.

Therefore, the result is only valid for small cross-sectional distances $z_1 - z_0 << 1$ and should be written in its infinitesimal form.

$$\frac{1}{K\kappa^2 \mathrm{Re}} \frac{\delta \xi}{\delta z} = \begin{bmatrix} -(1-\xi_1^2)(4-\xi_1^2)\cos\xi_2 \\ (4 - 23\xi_1^2 + 7\xi_1^4)\sin\xi_2 \end{bmatrix} + \mathcal{O}(\kappa) \tag{42}$$

Figure 30 presents the result graphically, where each vector represents the infinitesimal displacement over a longitudinal distance of dz. The biggest mixing is experienced by the points in the regions close to the wall at the top and the bottom.

Appendix B. Code

In this section the code used to create the bifurcation geometry is presented in cases the reader needs to duplicate the exact same geometry in this paper. The BifGeom.py contains methods and geom_client.py is a sample client that utilizes these methods to create the geometry. The files must be run from within CFD-GEOM by CFD Corporation.

```
import BifGeom

# H=0                                    - height, usually set to 0
# L=4                                    - length of the straight portions of the pipe
# r=0.5                                  - mother to daughter tube diameter ratio
# alpha_deg=120 - total bifurcation angle in degrees
# delta=1/N              - grid spacing

N = 25;

BifGeom.BuildGeom(0, 4, 0.5, 120, 1/N)
```

```
import math

import GPoint
import GCurve
import GEntity
import GSurface
import GCurve
import GManip
import GLoop
import GEdge
import GUnstruct
import GGrid

import GInterface

#compute a modified blending curve to avoid the angle of zero
def BlendCurve(LA, PA, LB, PB):
    r = 1.0/2.5
    curve = GCurve.CreateBlendCurve(LA, PA, LB, PB)
    op_spl1 = GManip.Split (curve, r, 1-r)
    op_spl2 = GManip.Split (op_spl1['curves'][1], (1-2*r)/(1-r), 1-(1-2*r)/(1-r))
    curve   = GCurve.CreateThroughPoints (PA, op_spl1['points'][0], op_spl2['points'][0], PB)
    return curve


#build geometry by manually giving radius of cuvature
# H          - height, usually set to 0
# L          - length of the straight portions of the pipe
# r          - mother to daughter tube diameter ratio
# alpha_deg - total bifurcation angle in degrees
# R_curv     - bifurcation curvature
# delta      - grid spacing

def BuildGeomR(H, L, r, alpha_deg, R_curv, delta):
```

```
alpha_deg = alpha_deg/2.0
R           = R_curv + 0.5


#computations
alpha    = alpha_deg*math.pi/180
C        = math.cos(alpha)
S        = math.sin(alpha)


#Creaet geometry
OO = GPoint.Create (0, H, 0)

circle0    = GCurve.CreateCircle (OO, 0.5)
circle1    = GManip.Split (circle0, 0.5, 0.5)
circle2    = GManip.Split (circle1[0], 0.5, 0.5)
circle3    = GManip.Split (circle1[1], 0.5, 0.5)

line_LA  =GCurve.CreatePtRevolvedCurve(circle0['points'][0], [ R, 0, 0],
                                                        [ R, 1, 0], alpha_deg )
line_LB  =GCurve.CreatePtRevolvedCurve(circle1['points'][0], [-R, 0, 0],
                                                        [-R, 1, 0],-alpha_deg )

line_CP = [circle2[1],circle3[0],circle3[1],circle2[0]]
line_CA = GManip.DuplAndRotate ([ R, 0, 0],[ R, 1, 0], alpha_deg, 1, line_CP)
line_CB = GManip.DuplAndRotate ([-R, 0, 0],[-R, 1, 0], -alpha_deg, 1, line_CP)


op_sclA = GManip.Scale ([r, r, r], [ R-C*R_curv, H, S*R_curv], line_CA)
op_scLA = GManip.Scale ([r, r, r], [-R+C*R_curv, H, S*R_curv], line_CB)

line_TP = GManip.DuplAndTranslate ([0, 0, -1], L, 1, line_CP)
line_TA = GManip.DuplAndTranslate ([ S, 0, C], L, 1, line_CA)
line_TB = GManip.DuplAndTranslate ([-S, 0, C], L, 1, line_CB)


line_LP0 = GCurve.CreateThroughPoints (circle2['points'][0], line_TP['points'][0])
line_LP1 = GCurve.CreateThroughPoints (circle1['points'][0], line_TP['points'][1])
line_LP2 = GCurve.CreateThroughPoints (circle3['points'][0], line_TP['points'][2])
line_LP3 = GCurve.CreateThroughPoints (circle0['points'][0], line_TP['points'][3])

line_LA0 = GCurve.CreateThroughPoints (line_CA['points'][0], line_TA['points'][0])
line_LA1 = GCurve.CreateThroughPoints (line_CA['points'][1], line_TA['points'][1])
line_LA2 = GCurve.CreateThroughPoints (line_CA['points'][2], line_TA['points'][2])
line_LA3 = GCurve.CreateThroughPoints (line_LA['points'][0],  line_TA['points'][3])

line_LB0 = GCurve.CreateThroughPoints (line_CB['points'][0], line_TB['points'][0])
line_LB1 = GCurve.CreateThroughPoints (line_LB['points'][0],  line_TB['points'][1])
line_LB2 = GCurve.CreateThroughPoints (line_CB['points'][1], line_TB['points'][2])
line_LB3 = GCurve.CreateThroughPoints (line_CB['points'][2], line_TB['points'][3])

lineAB = GCurve.CreateBlendCurve(line_LB3, line_CB['points'][2], line_LA1,
                                                             line_CA['points'][1])
lineAU = BlendCurve(line_LA0, line_CA['points'][0], line_LP0, circle2['points'][0])
lineAD = BlendCurve(line_LA2, line_CA['points'][2], line_LP2, circle3['points'][0])
lineBU = BlendCurve(line_LB0, line_CB['points'][0], line_LP0, circle2['points'][0])
lineBD = BlendCurve(line_LB2, line_CB['points'][1], line_LP2, circle3['points'][0])
lineUU = BlendCurve(line_LA0, line_CA['points'][0], line_LB0, line_CB['points'][0])
lineDD = BlendCurve(line_LA2, line_CA['points'][2], line_LB2, line_CB['points'][1])

#edges
NA = int(math.pi*r/delta)
NP = int(math.pi/delta)
NL = int(L/delta)
```

```
NO = int(alpha*R_curv/delta)
NI = int(alpha*R/delta)
NS = int(2.0*(R-C*(R_curv+r))/delta)


edge_CA0 = GEdge.CreatePowerLaw (line_CA[0], NA/4, 1, 1)
edge_CA1 = GEdge.CreatePowerLaw (line_CA[1], NA/4, 1, 1)
edge_CA2 = GEdge.CreatePowerLaw (line_CA[2], NA/4, 1, 1)
edge_CA3 = GEdge.CreatePowerLaw (line_CA[3], NA/4, 1, 1)

edge_CB0 = GEdge.CreatePowerLaw (line_CB[0], NA/4, 1, 1)
edge_CB1 = GEdge.CreatePowerLaw (line_CB[1], NA/4, 1, 1)
edge_CB2 = GEdge.CreatePowerLaw (line_CB[2], NA/4, 1, 1)
edge_CB3 = GEdge.CreatePowerLaw (line_CB[3], NA/4, 1, 1)

edge_CP0 = GEdge.CreatePowerLaw (line_CP[0], NP/4, 1, 1)
edge_CP1 = GEdge.CreatePowerLaw (line_CP[1], NP/4, 1, 1)
edge_CP2 = GEdge.CreatePowerLaw (line_CP[2], NP/4, 1, 1)
edge_CP3 = GEdge.CreatePowerLaw (line_CP[3], NP/4, 1, 1)

edgeUU = GEdge.CreatePowerLaw (lineUU, NI, 1, 1)
edgeAB = GEdge.CreatePowerLaw (lineAB, NS, 1, 1)
edgeDD = GEdge.CreatePowerLaw (lineDD, NI, 1, 1)

edgeAU = GEdge.CreatePowerLaw (lineAU, NI, 1, 1)
edge_A = GEdge.CreatePowerLaw (line_LA, NO, 1, 1)
edgeAD = GEdge.CreatePowerLaw (lineAD, NI, 1, 1)

edgeBU = GEdge.CreatePowerLaw (lineBU, NI, 1, 1)
edge_B = GEdge.CreatePowerLaw (line_LB, NO, 1, 1)
edgeBD = GEdge.CreatePowerLaw (lineBD, NI, 1, 1)

#loops
loops=[]

loops.append (GLoop.Create ([edge_CP0,edge_CP1,edge_CP2,edge_CP3]))
loops.append (GLoop.Create ([edge_CA0,edge_CA1,edge_CA2,edge_CA3]))
loops.append (GLoop.Create ([edge_CB0,edge_CB1,edge_CB2,edge_CB3]))


loops.append (GLoop.Create ([edge_CP3,edgeAU,edge_CA3,edge_A]))
loops.append (GLoop.Create ([edge_CP0,edge_B,edge_CB0,edgeBU]))
loops.append (GLoop.Create ([edge_CP1,edgeBD,edge_CB1,edge_B]))
loops.append (GLoop.Create ([edge_CP2,edge_A,edge_CA2,edgeAD]))
loops.append (GLoop.Create ([edge_CA0,edgeAB,edge_CB3,edgeUU]))
loops.append (GLoop.Create ([edge_CA1,edgeDD,edge_CB2,edgeAB]))
loops.append (GLoop.Create ([edgeUU,edgeBU,edgeAU]))
loops.append (GLoop.Create ([edgeDD,edgeBD,edgeAD]))



#surfaces
surfs=[]

surfs.append (GSurface.CreateFourSided (line_CP[0],line_CP[1],line_CP[2],line_CP[3]))
surfs.append (GSurface.CreateFourSided (line_CA[0],line_CA[1],line_CA[2],line_CA[3]))
surfs.append (GSurface.CreateFourSided (line_CB[0],line_CB[1],line_CB[2],line_CB[3]))

surfs.append (GSurface.CreateFourSided (line_CP[3],lineAU,line_CA[3],line_LA))
surfs.append (GSurface.CreateFourSided (line_CP[0],line_LB,line_CB[0],lineBU))
surfs.append (GSurface.CreateFourSided (line_CP[1],lineBD,line_CB[1],line_LB))
surfs.append (GSurface.CreateFourSided (line_CP[2],line_LA,line_CA[2],lineAD))
surfs.append (GSurface.CreateFourSided (line_CA[0],lineAB,line_CB[3],lineUU))
surfs.append (GSurface.CreateFourSided (line_CA[1],lineDD,line_CB[2],lineAB))
surfs.append (GSurface.CreateFourSided (lineAU,lineUU,lineBU))
```

```
    surfs.append (GSurface.CreateFourSided (lineAD,lineDD,lineBD))


    #trim
    for count in range(len(surfs)):
        GLoop.TrimSurface (surfs[count], loops[count])

    #create irregular domain
    surfset = GUnstruct.CreateClosedSurfaceSets (loops)
    domain = GUnstruct.CreateDomain (surfset['domains'][0])

    GGrid.SetSurfaceMeshingParameters(domain, 0, 30, 1.01, 10.0*delta, delta/10.0, 1)
    GUnstruct.GenerateTriangularMesh (domain)
    GGrid.SetTetMeshingParametersAndMesh(domain,0, 1, 1.01, 5.5, 0)

    #   extrude pipes
    extP = GGrid.ExtrudeBlocksAndPrismsAlongVector(loops[0], [ 0, 0,-1], L, NL, 1, 1, 1)
    extA = GGrid.ExtrudeBlocksAndPrismsAlongVector(loops[1], [ S, 0, C], L, NL, 1, 1, 1)
    extB = GGrid.ExtrudeBlocksAndPrismsAlongVector(loops[2], [-S, 0, C], L, NL, 1, 1, 1)

    GEdge.SetHyptan (extP['edges'][0], int(NL/4.0), delta  , 0.0 ,1)
    GEdge.SetHyptan (extA['edges'][1], int(NL/2.0), delta  , 0.0 ,1)
    GEdge.SetHyptan (extB['edges'][2], int(NL/2.0   ), delta  , 0.0 ,1)

    #BC
    GEntity.SetBC (extP['loops'][0], 'Inlet')
    GEntity.SetBC (extA['loops'][0], 'Outlet')
    GEntity.SetBC (extB['loops'][0], 'Outlet')

    GEntity.SetBCName (extP['loops'][0], 'in')
    GEntity.SetBCName (extA['loops'][0], 'outA')
    GEntity.SetBCName (extB['loops'][0], 'outB')

    GEntity.SetVCName (domain,'volT')
    GEntity.SetVCName (extP,  'volP')
    GEntity.SetVCName (extA,  'volA')
    GEntity.SetVCName (extB,  'volB')


#compute radius of curvature
def radius(r, alpha_deg):
    alpha_deg=alpha_deg/2.0
    C = math.cos(math.pi/180*alpha_deg)
    return (0.5+r*C)/(1-C)

#build geometry (curvature computed automatically)
def BuildGeom(H, L, r, alpha_deg, delta):
    loops = BuildGeomR(H, L, r, alpha_deg, radius(r,alpha_deg), delta)

#create geometry and save it as a dtf file for processing with CFD-ACE
def CreateGeometryOnce(L,r,alpha_deg,delta,filename):
    BuildGeom(0, L, r, alpha_deg, delta)
    GInterface.DTFWrite_3d(filename)
```

References

[1] SA BERGER, L. TALBOT, and LS YAO. Flow in curved pipes. *ANNUAL REVIEW OF FLUID MECHANICS*, 15(169):461–512, 1983.

[2] M. G. Blyth and A. J. Mestel. Steady flow in a dividing pipe. *JOURNAL OF FLUID MECHANICS*, 401(31):339–364, DEC 25 1999.

[3] I. Chatziprodromou, V. D. Butty, V. B. Makhijani, D. Poulikakos, and Y. Ventikos. Pulsatile blood flow in anatomically accurate vessels with multiple aneurysms: A medical intervention planning application of computational haemodynamics. *FLOW TURBULENCE AND COMBUSTION*, 71:333–346, 2003.

[4] D. N. Ku. Blood flow in arteries. *ANNUAL REVIEW OF FLUID MECHANICS*, 29:399–434, 1997.

[5] S. MURATA, Y. MIYAKE, and T. INABA. Laminar-flow in a curved pipe with varying curvature. *JOURNAL OF FLUID MECHANICS*, 73:735–752, 1976.

[6] RJ PEDLEY, RC SCHROTER, and MF SUDLOW. Flow and pressure drop in systems of repeatedly branching tubes. *JOURNAL OF FLUID MECHANICS*, 46(19):365–&, 1971.

[7] J. Ravensbergen, J. K. B. Krijger, B. Hillen, and H. W. Hoogstraten. Merging flows in an arterial confluence: The vertebro-basilar junction. *JOURNAL OF FLUID MECHANICS*, 304(23):119–141, DEC 10 1995.

[8] S. J. Sherwin, O. Shah, D. J. Doorly, J. Peiro, Y. Papaharilaou, N. Watkins, C. G. Caro, and C. L. Dumoulin. The influence of out-of-plane geometry on the flow within a distal end-to-side anastomosis. *Journal of Biomechanical Engineering*, 122(1):86–95, 2000.

[9] J. H. Siggers and S. L. Waters. Steady flows in pipes with finite curvature. *PHYSICS OF FLUIDS*, 17, JUL 2005.

[10] F. T. Smith and M. A. Jones. One-to-few and one-to-many branching tube flows. *JOURNAL OF FLUID MECHANICS*, 423:1–31, NOV 25 2000.

[11] FT SMITH. Entry-flow effects in bifurcating, blocked or constricted tubes. *JOURNAL OF FLUID MECHANICS*, 78(16):709–736, 1976.

[12] M. Tadjfar. Branch angle and flow into a symmetric bifurcation. *JOURNAL OF BIOMECHANICAL ENGINEERING-TRANSACTIONS OF THE ASME*, 126:516–518, AUG 2004.

[13] M. Tadjfar and F. T. Smith. Direct simulations and modelling of basic three-dimensional bifurcating tube flows. *JOURNAL OF FLUID MECHANICS*, 519:1–32, NOV 25 2004.